Review-article

Meteorol. Zeitschrift, N.F. 5, 4–23 (Februar 1996)

On conditions for contrail formation from aircraft exhausts

U. SCHUMANN, Oberpfaffenhofen

Summary. The formation of contrails (condensation trails) from aircraft exhaust has been investigated since 1919. Related studies are reviewed. The thermodynamical foundation of the Appleman threshold criterion for contrail formation has been first described by SCHMIDT in 1940. The Schmidt/Appleman criterion is reexamined, including the effects of the conversion of part of the combustion heat into kinetic energy of the motions in the wake of the aircraft causing higher threshold temperatures for contrail formation than without this conversion. The criterion is also derived including the kinetic energy of the jet plumes but this effect changes the threshold temperature only a little. The analysis is applied for a measured test case with the so-called ATTAS aircraft and for typical modern wide-body aircraft of type B747. If the aircraft would burn liquid hydrogen (liquid methane) instead of kerosene fuel, contrails would appear at typically 10 K (4.5 K) higher ambient temperatures and would be geometrically thicker and longer. However, this does not necessarily mean that such alternative fuels have a stronger impact on climate because such fuels will cause less and larger particles with smaller optical thickness and faster sedimentation.

Über Bedingungen zur Bildung von Kondensstreifen aus Flugzeugabgasen

Zusammenfassung. Die Bildung von Kondensstreifen aus Flugzeugabgasen wurde seit 1919 untersucht. Entsprechende Studien werden in einer Übersicht dargestellt. Die thermodynamische Grundlage der von Appleman angegebenen Grenzwert-Bedingung für die Bildung von Kondensstreifen wurde zuerst von SCHMIDT im Jahr 1940 beschrieben. Das Schmidt/Appleman-Kriterium wird dargestellt und erweitert. Die teilweise Umwandlung von Verbrennungswärme in kinetische Energie im Nachlauf eines Flugzeuges führt zu einer Erhöhung der Grenztemperatur zur Kondensstreifenbildung. Es wird auch untersucht, wieweit die kinetische Energie des Abgasstrahls der Triebwerke die Kondensstreifen verändert. Es zeigt sich, daß dieser Effekt die Grenztemperaturen für Kondensstreifen nur wenig verändert. Die Analyse wird angewandt auf Beobachtungen an dem sogenannten ATTAS Flugzeug und auf typische Großraumflugzeuge vom Typ B747. Bei Verwendung von flüssigem Wasserstoff (flüssigem Methan) statt Kerosin entstünden Kondensstreifen typisch bei 10 K (4.5 K) höheren Umgebungstemperaturen und die Kondensstreifen hätten größere Durchmesser und Längen. Daraus kann allerdings nicht auf größere Klimabeeinflussung geschlossen werden, da solche Kondensstreifen vermutlich weniger, aber größere Partikel mit geringerer optischer Dicke und rascherer Sedimentation verursachen.

1. Introduction

The clouds often visible to be formed in the wake of aircraft are called condensation trails (BREWER 1946) or contrails (APPLEMAN 1953). Contrails form for various reasons but the most important is the emission of water vapour. In order to form contrails, the air must be cold, typically colder than –40°C, but the precise threshold value depends on pressure, ambient humidity, the amounts of heat and water vapour released from the aircraft, and on details of the mixing and particle formation processes in the aircraft wake. These details are not yet fully understood. Because of the low temperature required, contrails form usually (outside polar regions) at high altitudes only. In recent years, the question how far contrails increase cloudiness and change the climatological or chemical state of the atmosphere triggered intensive research (SCHUMANN 1990, 1994; SCHUMANN and WURZEL 1994; WMO 1995). The explanation of how and when contrails form in the atmosphere is usually attributed to APPLEMAN (1953). However, studies on contrail formation go back to the year 1919 and much of the older literature seems to be overlooked. This paper reviews the history of contrail research and reexamines the thermodynamical conditions which have been deduced to explain how contrails form. This study was initiated by discrepancies found between observed and computed threshold conditions (BUSEN and SCHUMANN 1995). Here, we investigate the question whether the conversion of kinetic energy into heat along the mixing exhaust jets from an aircraft engine may contribute to explain observed differences. Moreover, the impact of alternative fuels, which are being considered for future aircraft (WINTER 1990), is discussed with respect to contrail formation. Figures 1 and 2 show examples of contrails which will be discussed in this paper.

2. Review of observations and explanations

Aircraft reached the altitudes required at midlatitudes for contrail formation in the period 1914–1919. Record flight altitudes reported for that time period are 6150 m (28. 12. 1913, E. LEGAGNEUX, France) and 9520 m (14. 6. 1919, Jean CASALE, France) (Fédération Aéronautique Internationale, Paris, personal communication 1995; ZFM 1914, 1920).

The first published report on contrail observations stems from ETTENREICH (1919). He observed 1915 in Southern Tirol "the condensation of a cumulus stripe from the exhaust gases of an aircraft" which was visible for a

0941-2948/96/0005-0004 $ 09.00

"long" time. Several eyewitness descriptions of "unusual clouds that were formed in the wakes of airplans" in 1918 have been commented by VARNEY (1921). Much attention was given to the contrails that formed over Munich on May 9, 11, and June 17, 1919, at flights by the pilot Zeno Diemer at altitudes up to 9300 m, first reported by WEICKMANN (1919). He observed a cloud stripe of about 50 km length forming structures that were attributed to vortex groups of the exhaust. Parts of a 22° halo were observed around the sun in the contrail as caused by a cloud of randomly oriented hexagonal ice prisms in contrails (LUDLAM and SCORER 1960, GREENLER 1980, TAPE 1994). The same event was commented upon by BASCHIN (1919), SCHREINER (1919), SCHMAUSS (1919), and WEGENER (1920).

In the time thereafter, this phenomenon received relatively little attention (PEPPLER 1930), until the detectability of aircraft became of obvious interest leading to several publications, including LÖHNER (1940), SCHMIDT (1941), AUFM KAMPE (1943), HEIËRMAN (1944), DESCAMPS (1945), BREWER (1946), and WEICKMANN (1945). A rather complete list of the resultant reports before 1951 was collected (133 entries) and shortly annotated by KRAMER (1951) with unpublished contributions by W. FINDEISEN, F. HÖHNDORF, H. J. AUFM KAMPE, and W. GEORGII in Germany, G. M. B. DOBSON, A. H. R. GOLDIE, H. HORROCKS, and A. E. PARKER in the UK, and R. V. RHODE and H. A. PEARSON in the USA in the years 1941–1943.

Although several authors pointed to the correct explanation early, the origin of contrails remained uncertain for a long time. Possible causes mentioned include emissions of water vapour, cloud-forming particles, and pressure reduction leading to saturation. Other, less likely or less important possibilities for contrail formation that have been suggested include shocks or vibrations from the engine (VARNEY 1921), effects connected with electrical charges (PEPPLER 1930), turbulence caused by propellers — leading to mixing layers of air (GOLDIE 1941, unpublished), and heat release triggering convective clouds (RHODE and PEARSON 1942, unpublished).

The possibility that the water vapour emitted from engines burning hydrocarbon fuels may cause supersaturation with respect to liquid water leading to cloud formation was considered early (HUMPHREYS, as discussed in VARNEY 1921), but for a long time not accepted as being reasonable because the ambient air was considered to be too dry to allow for cloud formation (PEPPLER 1930) and the amount of emitted water vapour appeared to be too small to explain the extended size of contrails sometimes observed. Moreover, it was known that very large supersaturations are required to form droplets or ice particles without suitable nuclei (VOLMER 1939, SIMPSON 1941, PRUPPACHER and KLETT 1980, p. 176). Therefore, several authors suggested that aircraft emit dust or soot particles from the engine exhaust providing sublimation nuclei for frost-supersaturated air, i.e. supersaturated with respect to ice but subsaturated for liquid water (WEICKMANN 1919, BASCHIN 1919, SCHMAUSS 1919, WEGENER 1920), or condensation nuclei in air supersaturated with respect to liquid water (SCHREINER 1919), or ions forming condensation nuclei (mentioned in LÖHNER 1940).

This wide variety of suggestions reveals the limited knowledge on cloud particle formation at that time. In the 40's evidence accumulated that sublimation nuclei are rare (WALL 1942; WEICKMANN 1945, 1949), while the atmosphere contains usually many (order 100 cm^{-3}) cloud condensation nuclei (CCN) to form droplets when slightly supersaturated with respect to the liquid phase (VOLMER 1939, SIMPSON 1941). The required supersaturation grows by the KELVIN (surface stress) effect and decreases for soluble matter in the nuclei by the Raoult (solute) effect (KÖHLER 1936). Computations showed that ice crystal nucleation requires higher supersaturation than liquid droplet nucleation, except for extremely low temperatures, although details of such computations remained uncertain because of unknown values of the energy of formation of ice crystals from the vapour phase (KRASTANOW 1940, WALL 1942). CCN may also result from small droplets formed by homogeneous binary nucleation of water vapour with gaseous sulphuric acid (MIRABEL and KATZ 1974) generated in the exhaust of engines burning sulphur containing fuel (REINER and ARNOLD 1993). Therefore, it is generally assumed that condensation starts to form water (or solution) droplets, not ice crystals, and if the temperature is below freezing point the droplets are supercooled (SCORER 1955). This was demonstrated very nicely by experiments with an expansion chamber at temperatures down to −50°C by REGENER (1941). He showed that even quartz crystals, which have a shape similar to the hexagonal form of ice crystals and which were expected to provide ice nuclei, first from droplets before getting frozen.

The phase of the particles is very important because ice particles in the contrails grow much faster than liquid droplets because of larger supersaturation. Supercooled pure water droplets freeze quickly at temperatures below a threshold temperature which may be as low as −45°C (PRUPPACHER 1995), especially in the young contrail with large cooling rates. Soluble matter depresses the freezing temperature (PRUPPACHER and KLETT 1980, p. 274–281). At higher temperatures, supercooled droplets may persist for some time, in particular when the droplets are small and free of any substrate causing immersion freezing. Therefore, contrail particles may stay liquid for some time but many of them if not all are expected to freeze within the life-time of contrails.

Hence, as summarized by HEIËRMAN (1944), DESCAMPS (1945), BREWER (1946), APPLEMAN (1953), SCORER (1955), and SCORER and DAVENPORT (1970), contrails originate, both for propeller and jet engine driven aircraft, from the emitted water vapour leading to condensation on nuclei preexisting or formed in the exhaust with subsequent freezing. The required water saturation is reached when the increase of water vapour concentration exceeds the increase in saturation water concentration with temperature due to simultaneous heat release, and this is the case only for sufficiently low temperature, the minimum (negative) trail temperature (MINTRA), decreasing with altitude. Con-

trails form early after the aircraft, see Fig. 1, and are short-lived when getting mixed with sufficiently dry ambient air.

Persistent trails, which do not evaporate when mixed with the environment, on the other hand, form when the ambient air is supersaturated with respect to ice, i.e. for frost saturation. Such conditions are not uncommon for the upper troposphere. Here, aircraft locally induce ice particles, presumably via the liquid phase, which then form the freezing nuclei necessary to trigger the formation of wide spreading ice cirrus layers often visible. The ice particles grow in size until all water vapour in excess of ice saturation has been deposited on the particles. The contrail then persists until its relative humidity drops below ice saturation (by mixing with dry ambient air, by subsidence or by radiative heating) or until the particles sediment into drier air (DETWILER and PRATT 1984). Such contrails may also develop into long-lasting subvisible cirrus cloud layers (SASSEN et al. 1989). Unfortunately, a climatology of the size, duration and frequency of regions with frost saturation does not exist. Persistent contrails have been observed to occur in particular ahead of frontal cirrus bands of warm fronts and at the southern side of jet streams but occur also in clear air remote from synoptic disturbances (CARLETON and LAMB 1986, BAKAN et al. 1994), presumably because of rising motion. In clear air, vertical motions may be caused by gravity waves. Upward motion carries more humid air upward and cools by adiabatic expansion, reaching ice saturation before reaching water saturation, and the altitude difference between these levels is about 300 m at $-40°C$ (DETWILER and PRATT 1984).

Aircraft may also induce ice particles in clouds containing supercooled droplets (RANGO and HOBBS 1983, 1984; KELLY and VALI 1991; SASSEN 1991; WOODLEY et al. 1991) and change the particle spectrum in natural cirrus (ALHEIT 1995), but we concentrate on contrails forming in clear air.

Contrails may also form at higher temperatures, even above 0°C, by aerodynamic effects. PARKER (1943, unpublished) computed the pressure reduction on the upper surface of wings, which is maximum near the leading edge.

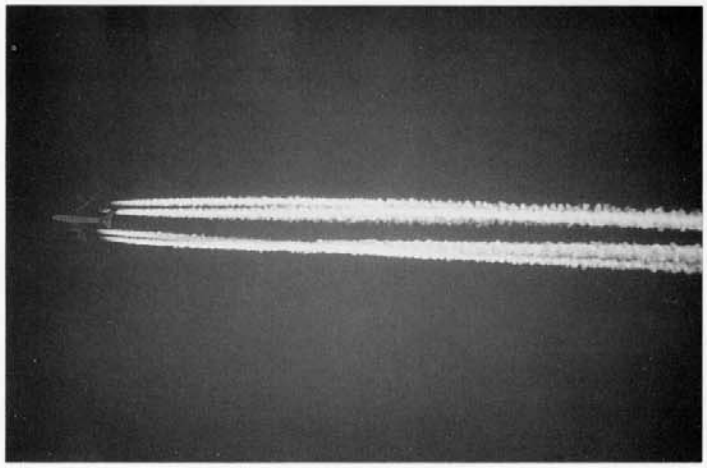

Fig. 1. Contrails behind a four engine jet airliner at cruise (Photo: R. ALHEIT).

Abb. 1. Kondensstreifen hinter einem vierstrahligen Verkehrsflugzeug im Reiseflug (Photo: R. ALHEIT).

Fig. 2. Contrails from a B747 aircraft seen from the research aircaft Falcon (Photo: H. ZIEREIS).

Abb. 2. Kondensstreifen eines B747 Flugzeugs aus der Sicht des Forschungsflugzeugs Falcon (Photo: H. ZIEREIS).

He concluded that the pressure drop is too small or lasts too short a time (order 0.02 s) to be important for contrail formation. He noted that trailing vortices are formed from the circulation around wings and propeller blades with maximum pressure reduction at the wing or blade tips causing adiabatic cooling. However, this effect is important only when the air is frost-saturated or contains supercooled cloud droplets (WOODLEY et al. 1991), because otherwise the tip trail evaporates quickly. Tip trails are observed at low altitudes in humid air (photos of wing trails in LUDLAM and SCORER 1960, p. 77; propeller trails in SCORER 1972, p. 121). Moist jet plumes which are captured in the trailing vortex system (visualized in CHIGIER 1974 and VAN DYKE 1982, photo no. 85 and 86) experience an additional adiabatic cooling due to the pressure drop within the vortices (MIAKE-LYE et al. 1993). This effect is the stronger the faster the aircraft, the shorter the wing span, and the closer the engine plumes are to the vortex axis. It is a small effect for subsonic aircraft but may be relevant for supersonic aircraft.

It took a rather long time to develop the thermodynamical theory required to predict the threshold condition for contrail formation from condensing exhaust water. Early studies considered the emitted water but ignored the heat release from the engines which reduces the relative humidity. Apparently, HÖHNDORF (1939) was the first who understood that contrail formation depends on both the water and heat release and showed that contrails form only above a certain threshold temperature, of −40°C at 10 km altitude. DOBSON and PARKER (1941–1943, unpublished) came to the same conclusions independently.

SCHMIDT (1941) and later APPLEMAN (1953) deduced a thermodynamical theory, which showed that the threshold conditions depend only on ambient pressure, humidity and the ratio of water and heat released into the exhaust plume. SCHMIDT (1941) used the MOLLIER i–x-diagram (MOLLIER 1923) in which isobaric mixing between two states of specific enthalpy i and water content x per unit mass of dry air follows along straight lines. As will be explained in section 3, mixing of the aircraft exhaust follows along the line connecting the states of the exhaust gas just after engine exit and in the environment. Contrails form when the mixing line penetrates the saturation curve. The threshold temperature beyond which saturation is reached is a function of pressure or altitude and relative humidity in the ambient air. In cold air, contrails form even for perfectly dry ambient atmosphere. SCHMIDT (1941) assumed that contrails form under equilibrium conditions when reaching ice saturation. HÖHNDORF (1941, unpublished) applied SCHMIDT's theory to saturation with respect to liquid water which explained contrail observations better. He noted that contrails grow fast after onset and this can be explained by freezing of liquid particles.

SCHMIDT (1941) also explained differences in contrail formation for different aircraft conditions by the fact that only part of the combustion heat is given directly to the exhaust gas depending on the aircraft performance. The other part is released to the ambient air in the form of radiation or kinetic energy of, e.g. turbulence and trailing vortices. This energy gets dissipated by turbulent and viscous mixing and warms the moist plume at later distance from the aircraft so that the early exhaust plume is cooler than to be expected from the total amount of combustion heat. As a consequence, the threshold temperature for contrail formation is higher than when the exhaust gases receive all combustion heat directly. APPLEMAN (1953) deduced essentially the same results for liquid saturation, but his derivation is given in a more pragmatic form.

In order to test the thermodynamic theories, extensive observations were performed by AUFM KAMPE (1942, 1943) and HORROCKS (1941–1942, unpublished). These observations corroborated the existence of threshold temperatures as a function of aircraft parameters. AUFM KAMPE (1942) observed that contrails disappear when the engine power gets reduced. Such power reduction reduces immediately the amount of water vapour release while the amount of heat release remains relatively large because of contributions from the hot engine with large heat capacity. Since the engine emits some exhaust particles even at idle, the observations support the conclusion that contrails form from water vapour emissions and not from emissions of condensation nuclei. This conclusion was further supported by the fact that seeding clear air at low temperatures with pulverized quartz did not trigger ice cloud formation although flying in regions where persistent contrails formed. AUFM KAMPE (1942, 1943) also performed in-situ measurements of the temperature in the wake of an aircraft at altitudes of 8–10 km. Measurements in the propeller wake 1.5 and 8.5 m after the engine were performed using thermometers mounted to the aircraft itself; measurements at 18.5–65.5 m distance were taken from a second aircraft towed with the first one. He computed the humidity increase from the known amount of fuel consumption and resultant water vapour emission for an estimate of the mixing cross-section of the exhaust plume. Contrail formation was found typically 10–20 m after the aircraft tail in agreement with computations assuming liquid saturation. Moreover, frost was observed to form on a towed body in the wake of the contrail-forming aircraft at distances of a few 100 m, indicating accretion of supercooled liquid droplets. Finally AUFM KAMPE (1942) applied the theories as developed by KRASTANOW (1940) and showed that droplet nucleation occurs before ice particles can form.

The existence of the threshold temperatures was confirmed also by observations of contrails on the ground in Canada and Alaska when the temperature was below −30°C (BREWER 1946, MURCRAY 1970), similar to ice-fog (THUMAN and ROBINSON 1954). Observations also showed a shortening of contrails in the stratosphere which coud not be explained by temperature changes alone. BREWER (1946) developed an air-borne frost-point hygrometer to measure the water vapour content during various high-altitude flights. These observations led to the detection that the stratosphere is much drier than the troposphere (DOBSON et al. 1946). BREWER (1946) also supported the explanation for persistent contrails by showing measured examples of frost-saturated air where the frost-point was several degrees

above ambient temperature and where persistent contrails were observed. These seem to be the only published measurements of such kind.

The project Cloud Trail (AWS 1956, 1981) presented statistics based on contrail observations obtained over 23 upper-air sounding stations in the USA. The results were presented as contrail frequencies versus temperature at various pressure levels, and as lines of constant contrail probability in a pressure-temperature diagram for various seasons. The project also collected data on cirrus and turbulence occurrences (AWS 1956).

JIUSTO and PILIÉ (1964) reviewed the principles of contrail formation and developed forecast rules for predicting the occurrence of contrails and their persistence. They estimated the relative humidity in areas without measurements (40 % in the upper troposphere, 0 % in the stratosphere, 50 % near the tropopause when the flow is from a moist region and 0 % from a dry region, 60 % when cirrus clouds are present), and identified regions which are favourable for contrail formation: 1. low-pressure areas in the upper troposphere and high-pressure areas in the lower stratosphere (related to vertical motions); 2. entire 200 hPa level in winter; 3. north of 35°N in winter and north of 60°N in summer at 300 hPa; 4. on the right side of jet streams looking downstream, up to 700 km from the axis; 5. 600 m up and down from the tropopause level; 6. areas where cirrus clouds are present. Latitude, altitude and season regions for contrails are also discussed in DOWNIE and SILVERMAN (1957), CIAP (1975), APPLEMAN (1957), DETWILER and PRATT (1984), and MIAKE-LYE et al. (1993). Examples of contrail observations from space are depicted in SCORER (1986) with some explanation of the responsible meteorology. Regional contrail statistics derived from satellite data can be found in CARLETON and LAMB (1986), DEGRAND et al. (1990), ROLL (1990), SCHUMANN and WENDLING (1990), and BAKAN et al. (1994).

Recently, PETERS (1993) performed an extensive study to verify and extend contrail-forecasting techniques. Contrail observations were collected from various jet aircraft for one year, with 4387 observations below 12 km altitude (40 000 feet) and 1040 observations above that altitude up to about 20 km. The observations were taken mainly over the USA with the bulk over California. Contrails were observed to occur at altitudes as low as 3 km. Flights above 10.7 km caused contrails in more than 50 % of all cases, and in 85 % of all cases at 12 km altitude. Flights in air warmer than −40°C caused contrails in less than 20 % of all flights, but the fraction exceeded 73 % below −51°C. The correlation between contrail occurrence and synoptic-scale vertical motions was analyzed using 300 hPa geopotential maps of trough-ridge patterns. Upward motion was assumed to exist between the base (southern edge, on the northern hemisphere) of a trough and the apex (northern edge) of the upstream (eastern) ridge, i.e. at the eastern side of cyclones. Downward motion was assumed to exist between the apex of the ridge and the base of the upstream trough, i.e. at the western side of anti-cyclones. The chances for contrail formation is about twice as high in areas with upward motion, presumably because of larger relative humidity. Comparisons to the Appleman method were made assuming relative humidity of 40 % in the troposphere, 70 % near the tropopause, and 10 % in the stratosphere. For data below 12 km altitude, this method explains 98 % of cases without contrails but only 27 % of cases with contrails. Hence, it underestimates the occurrence of contrails in the troposphere. PETERS (1993) explained this discrepancy with the lower heat emission per emitted mass of water vapour of modern high-bypass engines and introduced engine specific corrections. The revised version predicts correctly 71 % of contrail occurrence and 82 % of non-occurrence for a high-bypass engine, while the Appleman criterion performance was only 35 and 37 %, respectively. The need for better humidity data was stressed. Unfortunately, the data were not classified into short-lived or persistent contrails.

BUSEN and SCHUMANN (1995) also observed short-lived contrails at temperatures significantly above the Appleman threshold temperature. They explained this apparent discrepancy (without knowing the work of SCHMIDT) with a fraction η of the combustion heat given to the trailing vortex system in terms of kinetic energy. They identified this fraction with the overall propulsion efficiency of the aircraft which depends on aircraft engine and flight parameters,

$$\eta = FV/(Q\dot{m}_F), \tag{1}$$

i.e. the amount of work performed against the aircraft drag compared to the amount of combustion heat, as a function of thrust F, true air speed V, specific combustion heat Q, and rate of fuel flow $\dot{m}_F$. The value of η of modern bypass turbofan engines (0.3 to 0.4) is higher than for older no-bypass turbojet engines or turbofan engines with low bypass ratio (Hagen 1982). In fact, the propulsion efficiency accounts for the same changes that were covered with engine-specific emission parameters by PETERS (1993) but η accounts not only for the engine performance but also for the aircraft speed and drag.

3. The Schmidt/Appleman theory

The Schmidt/Appleman theory is derived and reexamined in this chapter. For this purpose, we express the water and heat content of air in terms of m and h, the specific water mass and enthalpy per mass of moist air, which are conserved under isobaric and adiabatic conditions (SCHMIDT 1963, IRIBARNE and GODSON 1981). Differences such as $\Delta m = m_P - m_E$ refer to the plume and environmental values. In this section, we assume stagnant exhaust plumes so that all jet energy is converted to internal energy (or enthalpy) of the plume gases.

Aviation fuels consist of molecules containing mainly carbon and hydrogen. Burning such fuel with air results in EI_{H_2O} mass units of water vapour per unit mass of fuel, where EI_{H_2O} is the so-called emission index for water vapour. It can be computed for various fuels as explained in Appendix 1 and listed in Table 1. Burning of one mass unit

of fuel with (N-1) mass units of air results in N mass units of exhaust gases. We call N the dilution factor. The water vapour in the exhaust gases mixes with air from the environment and adds to its water content m_E. As a result, the exhaust in the plume contains m_P mass fractions of water vapour, where

$$m_p = \frac{EI_{H_2O} + (N-1)m_E}{N} \quad \text{or} \quad \Delta m = m_p - m_E = \frac{EI_{H_2O} - m_E}{N}. \tag{2}$$

Simultaneously, the engine releases the combustion heat Q per mass of fuel from burning fuel with air. Values of Q for various fuels are given in Table 1, see also Appendix 1. As explained above, a fraction η of the combustion heat is converted into work to propel the aircraft. Hence, the exhaust gases take up the heat $(1-\eta)Q$ per mass of fuel. We ignore heat losses due to incomplete combustion and assume that heat and water are added to the plume and mix similarly, i.e. with equal diffusivities and similar initial conditions. This requires quick mixing of the moist core jet with the dry bypass jet of modern jet engines.

Just as the water mass, the combustion heat adds to the heat content (enthalpy) h_E of the air burnt which the fuel or mixed with the exhaust. The specific enthalpy of the exhaust plume gases is h_p,

$$\Delta h = h_p - h_E = \frac{Q(1-\eta) - h_E}{N}. \tag{3}$$

During mixing of the exhaust gases with ambient air, the dilution factor N increases without limit. In the absence of other heat losses or additions (such as due to radiation or expansion of the gases against a changing exhaust pressure), i.e. under adiabatic and isobaric conditions (with respect to the system containing the exhaust and the air mixed into the plume), Eqs. (3) and (2) are satisfied for all values of N. Since the ambient mass and heat contents m_E and h_E are small compared to EI_{H_2O} and Q, we may use the approximation

$$\Delta m = EI_{H_2O}/N, \quad \Delta h = Q(1-\eta)/N. \tag{4}$$

Hence, the mixing follows along a straight line $h_p(m_p)$ in an h–m diagram from the conditions immediately after the engine to the state h_E, m_E in the ambient air.

In general, the specific enthalpy is a function of temperature, pressure, composition and phase of the constituents (SCHMIDT 1963). MOLLIER (1923) provided diagrams of the enthalpy for given temperature as a function of water concentration assuming thermodynamic phase equilibrium at constant pressure, and SCHMIDT (1941) extended such diagrams to low temperatures. The specific enthalpy of engine exhaust gases is tabulated in HAGEN (1982). For ideal gases, the specific enthalpy is a pure function of temperature T,

$$h - h_E = \int_{T_E}^{T} c_p dT, \tag{5}$$

with $c_p(T)$ as specific heat capacity at constant pressure. The value of c_p depends on the temperature and the composition of the exhaust gases. The non-air exhaust components can be neglected for large dilution N and small ambient water vapour content m_E, but $c_p(T)$ varies, for dry air, between 1001.5 J kg^{-1} K^{-1} for T = 200 K and 1050 J kg^{-1} K^{-1} for T = 600 K, which is typically the exhaust gas temperature at the core exit of modern jet engines (HAGEN 1982). Only for large dilution, when the plume temperature has dropped below about 50°C, a constant value $c_p \equiv 1004$ J kg^{-1} K^{-1} may be used.

The water concentration m_p is related to the partial pressure e_p of vapour in the plume by

$$m_p = \frac{R_{air}}{R_{H_2O}} \frac{e_p}{p} = \varepsilon \frac{e_p}{p}, \tag{6}$$

as a function of total air pressure p and the ratio of gas constants or molar masses of dry air and water vapour, $\varepsilon = M_{H_2O}/M_{air} = 0.622$. Hence, the partial pressure e_p of water vapour and the temperature T_p in the plume are related by

$$\frac{\Delta e}{\Delta T} = \frac{e_p - e_E}{T_p - T_E} = G, \tag{7}$$

with the important parameter

$$G = \frac{EI_{H_2O} c_p p}{\varepsilon Q(1-\eta)}. \tag{8}$$

Throughout the mixing process, the dilution factor satisfies

$$N = EI_{H_2O}/\Delta m = Q(1-\eta)/\Delta h \equiv Q(1-\eta)/(c_p \Delta T), \tag{9}$$

where the last relation assumes a constant value of c_p and gaseous state. Hence, for sufficiently low temperatures and without phase change, mixing follows a line in the e_p–T

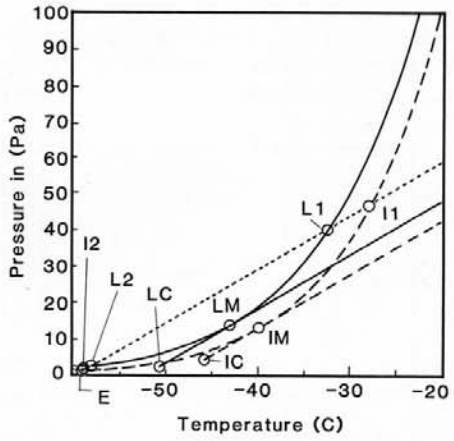

Fig. 3. Water vapour partial pressure versus temperature with saturation for liquid water (full curve) and ice (dashed), and lines of isobaric mixing for contrail onset at liquid saturation (full), ice saturation (long-dashed) and ambient temperature (short-dashed). The various points are discussed in the text.

Abb. 3. Partialdruck von Wasserdampf als Funktion der Temperatur mit Sättigungsdruck für flüssiges Wasser (volle Kurve) und Eis (gestrichelt) und Geraden der isobaren Mischung in den Fällen von Kondensstreifenbildung bei flüssiger Sättigung (voll), Eissättigung (lang strichliert) und bei Umgebungstemperatur (kurz gestrichelt). Die ausgezeichneten Punkte werden im Text diskutiert.

diagram as plotted in Fig. 3. Here each point corresponds to a specific value of N. The gradient of the mixing line is G. The engine conditions are on the far right upper corner outside the range plotted.

In the same diagram, we have plotted the saturation pressures of liquid water $e_L(T)$ and ice $e_I(T)$ for plane surfaces (SONNTAG 1994). The use of partial pressure instead of water mass fraction has the advantage that the saturation curves remain invariant under changes in air pressure p, but the steepness G of the mixing line increases with p. We see that the mixing line may cross the liquid (ice) saturation curve if the ambient temperature T_E is lower than the threshold temperature T_{LC} (T_{IC}). (We consider the ice and liquid saturation cases simultaneously for completeness.) Under threshold conditions, i.e. for $T_E = T_{LC}$ (T_{IC}), the mixing line just touches the saturation curves at T_{LM} (T_{IM}),

$$\frac{de_L(T_{LM})}{dT} = G, \quad \frac{de_I(T_{IM})}{dT} = G. \tag{10}$$

The values of T_{LM} and T_{IM} can be computed as explained in Appendix 2. They depend on G, and hence on the fuel parameters, the propulsion efficiency, and the ambient pressure.

Because of Eq. (7), with differences between states LM and LC (IM and IC), where $e_E = Ue_L(T_{LC,IC})$ is the vapour pressure in the environment under threshold conditions, the threshold temperatures T_{LC} and T_{IC} follow from

$$T_{LC} = T_{LM} - [e_L(T_{LM}) - Ue_L(T_{LC})]/G, \tag{11}$$

$$T_{IC} = T_{IM} - [e_I(T_{IM}) - Ue_L(T_{IC})]/G. \tag{12}$$

In general, these are implicit equations requiring numerical solutions by Newton iteration (suitable initial guesses are given in Appendix 2), depending on the relative humidity U of the ambient air. For U = 1, $T_{LC,IC} = T_{LM,IM}$, and minimum values are obtained explicitly for U = 0. The threshold temperature T_{LC} can be presented as in Fig. 4, the so-called Schmidt-Appleman diagram, as a function of ambient pressure p or altitude for given relative ambient humidity U, together with a standard temperature profile (NASA 1976).

Fig. 4a shows T_{LC} versus altitude for three values of ambient relative humidity, for kerosene fuel (Table 1) and $\eta = 0.3$. In regions of low temperature (to the left of the dashed curve, for U = 0), aircraft induce contrails even in perfectly dry air. For ambient temperatures between the T_{LC}-values for zero and 100 % relative humidity, contrails form if the ambient humidity exceeds the respective value. For ambient temperatures above T_{LM}, i.e. T_{LC} for 100 % relative humidity, aircraft do not lead to water saturation. Hence contrails are not expected to occur here. For the standard atmosphere shown in Fig. 4, contrails form above 8.4 km and, for typically low stratospheric humidity, below 14 km altitude. Persistent contrails are expected to form in regions where contrails lead to water saturation and where the ambient humidity exceeds ice saturation. This is possible everywhere for temperatures below T_{LM}. If persistent contrails would be observed to form above T_{LM}, then this would be a strong indication that contrails are formed from ice deposition nuclei. However, we do not know of such observations. Above T_{IM}, aircraft dissipate ice clouds.

Earlier onset of contrails is to be expected when using liquid hydrogen or liquid methane as fuel. As can be seen comparing Fig. 4b and 4a, hydrogen fuels lead to typically 10 K higher threshold temperatures. Under standard atmospheric conditions, such contrails could occur above 6.3 km and below 19.5 km altitude. For liquid methane, contrails are to be expected at 4.5 K higher temperatures compared to kerosene. On the other hand, less contrails are to be expected when using fuels with low hydrogen content.

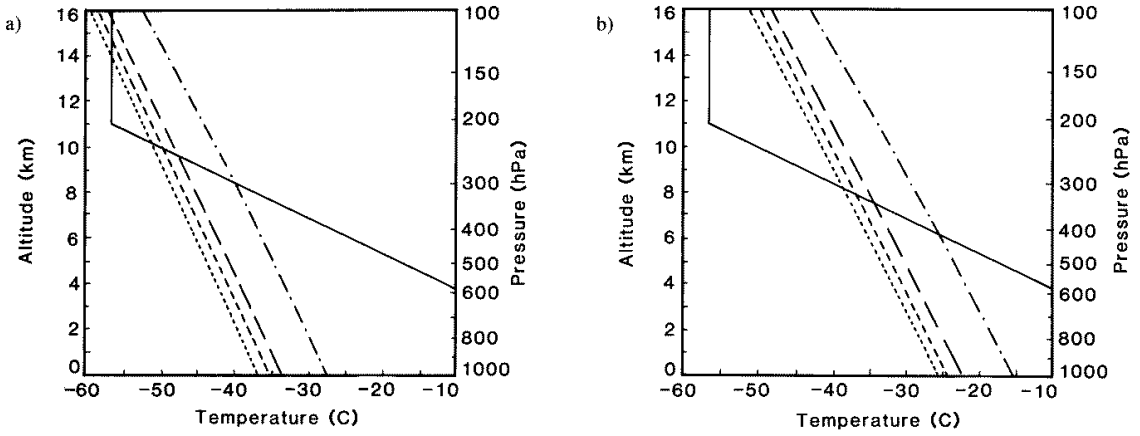

Fig. 4. Schmidt-Appleman diagram with threshold temperature T_{LC} versus altitude for relative humidity of 0 (short-dashed curve), 30 % (medium-dashed), 60 % (long-dashed) and 100 % (dash-dotted line), and the temperature profile of the international standard atmosphere (full). (a) For kerosene and overall propulsion efficiency of 0.3, (b) for hydrogen fuel and same efficiency.

Abb. 4. Schmidt-Appleman Diagramm mit Grenzwert-Temperatur T_{LC} als Funktion der Höhe für relative Feuchten von 0 (kurze Striche), 30 % (mittlere Striche), 60 % (lange Striche) und 100 % (strichpunktierte Kurve), sowie das Temperaturprofil der internationalen Standardatmosphäre (voll).

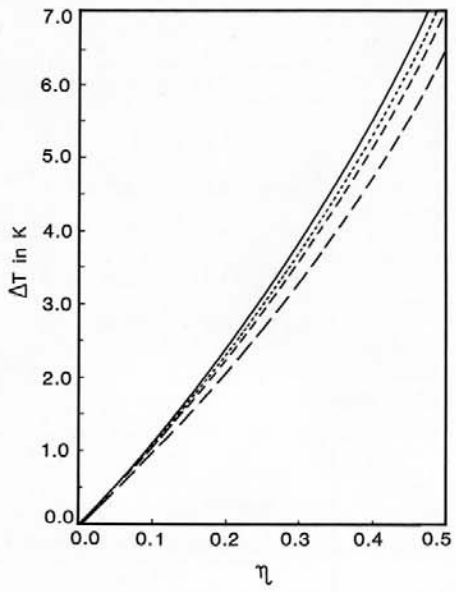

Fig. 5. Increase in threshold temperature with propulsion efficiency η for 100 % relative ambient humidity and pressure of 100 (long-dashed) and 400 hPa (full curve), with curves for 200 and 300 hPa between.

Abb. 5. Zunahme der Grenzwert-Temperatur mit dem Antriebswirkungsgrad η für 100 % relative Feuchte in der Umgebung mit Drücken von 100 (lang gestrichelt) und 400 hPa (volle Kurve), mit Kurven für 200 und 300 hPa dazwischen.

Fig. 5 shows that the critical temperature increases with η by about 1.4 K per 10 % increase in efficiency. This result is fairly insensitive to ambient pressure, humidity and the type of fuel. Hence, modern aircraft with high propulsion efficiency cause contrails at lower altitude than older aircraft. For 10 % higher efficiency and the standard atmospheric profile, contrails may occur at about 280 m lower altitude in the troposphere and at 800 m higher altitude in the stratosphere.

Obviously, contrails form only when the gradient of the saturation pressure with temperature is less than G, which requires $T_E<T_{LM}$. Otherwise, the engine adds more heat than moisture and reduces the relative humidity in the plume compared to environmental air. Therefore, aircraft may also lead to dissipation trails or "distrails" (BREWER 1946) by evaporating clouds along the flight path (BASCHIN 1919, KÜTTNER 1946), see photo in LUDLAM and SCORER (1960), p. 78. Distrails may also form by aircraft-induced mixing of cloudy air with drier air (SCORER 1972, p. 121).

For sufficiently low temperatures, the mixing line cuts through the saturation curves, see Fig. 3. The hot and moist exhaust plume leaving the engine gets diluted and reaches saturation, first at point I1 for ice saturation. Without phase change mixing continues along the mixing line and reaches L1 for water saturation, passes above points IM and LM of maximum ice and liquid supersaturation, then dilutes further to reach again saturation for liquid water (L2) and ice (I2) until it approaches the ambient conditions E. The points L1 and L2 (I1 and I2) exist if $T_E<T_{LC}$ ($T_E<T_{IC}$), and are determined by

$$e_L(T_{L1,L2}) - e_E = G(T_{L1,L2} - T_E), \tag{13}$$

$$e_L(T_{I1,I2}) - e_E = G(T_{I1,I2} - T_E), \tag{14}$$

with $e_E = Ue_L(T_E)$.

With phase change, the mixing approaches the respective saturation curve, e.g. for liquid saturation, condensing m_L of water per unit mass of plume air. This amount is smaller than the amount $m_0 = \varepsilon[e_p - e_L(T_p)]/p$ of water above saturation, because release of latent heat L_v (2.635 MJ kg^{-1} at −50°C) per unit mass of water vapour causes a slight increase in temperature (IRIBARNE and GODSON 1981, p. 130). With a change in water vapour concentration due to phase change, the enthalpy differential satisfies $dh = c_p dT + L_v dm$. Hence, the condensation of m_L of water at constant enthalpy causes an increase in temperature of about $\delta T = m_L L_v/c_p$. The small temperature increase reduces the amount of liquid water available according to the change in saturation water vapour with δT, $m_L = m_0 - \delta T\varepsilon(de_L/dT)/p$. As a consequence,

$$m_L = \frac{\varepsilon}{p}\frac{e_p - e_L}{1+\alpha_L}, \quad \alpha_L = \frac{\varepsilon}{p}\frac{L_v}{c_p}\frac{de_L}{dT}. \tag{15}$$

At point LM, $de_L/dT = G$, so that

$$\alpha_{LM} = \frac{EI_{H_2O}L_v}{Q(1-\eta)}. \tag{16}$$

For parameters as given in Tables 1 and 2, numerical values of α_{LM} are listed in Table 3. For kerosene, about 90 % of the available water may condense. For ice formation one has also to consider the latent heat of sublimation.

Visibility requires a certain amount of condensed water r_{min} per unit volume, depending on the contrail diameter, particle size spectrum, viewing angle with respect to the sun, and background, see Appendix 3. Therefore, the effective threshold temperature is slightly smaller and can be computed as above with saturation pressure enlarged by $e_{min} = r_{min}p(1 + \alpha_L)/(\varepsilon\rho)$ with air density ρ (APPLEMAN 1953, IRIBARNE and GODSON 1981, p. 135).

Because of quicker mixing, saturation is reached earlier at the outer edge of the plume than in the centre (DOWNIE and SILVERMAN 1957, CIAP 1975, KÄRCHER 1994, SCHUMANN et al. 1996). However, each plume parcel goes through the same mixing states as long as heat and water mix similarly. As an approximation, one may assume that all emissions mix at the same rate with the environment regardless of the radial distance from the plume axis. Then one can relate the plume cross-section area A and its diameter $D = (4A/\pi)^{1/2}$, for given fuel mass flow rate $\dot{m}_F$ and speed of aircraft V, with the dilution factor N,

$$\rho AV = \dot{m}_F N. \tag{17}$$

Here $\rho = p/(R_{air}T_p)$ is the plume gas density. Finally, we can estimate the plume jet velocity V_j relative to ambient air. Just as water emissions and enthalpy, the exhaust gases

within a plume cross-section A have to take up the momentum of the jets leaving the engines. The rate of momentum change per flight distance in the plume is ρAVV_j. This momentum change equals the thrust F from the engine on the aircraft. Hence,

$$V_j = F/(\rho AV). \quad (18)$$

These equations may be used to compute the jet speed together with the diameter, the temperature, the water content and the corresponding supersaturation, e.g. over liquid water $S = (e_p - e_L)/e_L$, in the mixed plume for given values of dilution N. For constant diffusivities, the cross-section area of a moving point source grows linearly with time. Hence, N represents qualitatively a nondimensional plume age.

4. Tests and parameter studies

BUSEN and SCHUMANN (1995) observed onset of contrail formation from the jet aircraft ATTAS at $p = 302.3 \pm 0.7$ hPa, $T_E = -49.7 \pm 0.5$°C, relative humidity of 34 % (possibly 45 %), for fuel with $Q = 43$ MJ kg^{-1}, $EI_{H_2O} = 1.21$, aircraft speed $V = 115$ m s^{-1}, fuel flow rate $\dot{m}_F = 0.125$ kg s^{-1}, and thrust $F = 6400 \pm 100$ N per engine, giving a propulsion efficiency of $\eta = 0.14 \pm 0.005$. For these conditions, we compute $T_{LC} = -50.4$°C. This value agrees with T_E within the experimental uncertainty of the observation. The contrail became visible in spite of the very small amount of water available. Actually one computes a maximum relative humidity of only 94.1 % in the plume. Slightly altered values, $T_E = -50.2$°C, and 45 % relative humidity, within the experimental uncertainty, result in $T_{LC} = -49.8$°C and a slight supersaturation of $S_{LM} = 3.2$ %. For $\eta = 0$ instead of 0.14, the threshold temperature would be 2 K smaller, about −51.8°, definitely below the observed ambient temperature. The computed plume diameters at the various mixing conditions for the higher supersaturation are 3.2, 3.7 and 10.6 m, at points L1, LM, and I2, which are consistent with the observed values. Hence, the threshold conditions fit the criterion for the given propulsion efficiency of the observed aircraft. It should be noted, however, that this agreement between observation and the revised Schmidt-Appleman criterion is perhaps incidental, since it is not yet understood how contrails can become visible shortly after the engine exit as observed without stronger supersaturation (KÄRCHER et al. 1995).

The same kind of analysis has been applied recently to determine the contrail dimensions in a second ATTAS experiment (SCHUMANN et al. 1996), where the contrail diameters could be measured with high accuracy. It has been found that the computed values agree within 20 % with the observed plume diameters.

In order to give an example of the resultant contrail parameters for a modern wide body aircraft, we evaluate the contrail conditions for the fuels and aircraft parameters as listed in Tables 1 and 2. The aircraft parameters of Table 2 correspond to observations taken at 15 UTC 13 November 1994 near 10°W, 51°N of an eastbound B747 with CF6-80C2B1F engines at 11.3 km altitude, just below the tropopause. The thrust and fuel flow values refer to one of the four engines. The thickness of the contrails depends on the fuel consumption. For comparison, we assume that the fuel flow rate follows from $\dot{m}_F = FV/(Q\eta)$ for otherwise fixed parameters, and hence is smaller for hydrogen than for kerosene fuel. The resultant parameters of the contrails are listed in Table 3. The mixing line as shown in Fig. 3 applies to the aircraft parameters as given in Table 2. For hydrogen, the mixing line is much steeper (see values of G in Table 3), causing higher values of T_{LM}.

From Table 3 we see that contrails start to form in the warm exhaust plume at temperatures which are considerably higher than ambient. The point of maximum water supersaturation LM is reached when the exhaust is diluted by a factor of the order 2000 relative to unit mass of fuel. The contrails form with initial plume diameters (from a single engine) of 3–4 m, and sublimate when mixed to diamters d_{I2} of more than 30 m. As expected, the plume diameters grow, see Table 3, with increasing EI_{H_2O}/Q. This value is 2.57 larger for hydrogen fuels than for kerosene, see Table 1.

The photo in Fig. 1 shows a four-engine airliner, with the silhouette (GREEN and SWANBOROUGH 1991) of a B747-200, at typical cruise conditions, near 11°E, 48°N, 12 UTC 11 March 1995 (at unknown altitude), when the air tempera-

Table 1. Fuel parameters.

Tabelle 1. Treibstoffparameter.

Fuel		Kerosene	Methane	Hydrogen
Nominal composition		$CH_{1.94}$	CH_4	H_2
Hydrogen mass fraction, m_H	kg kg^{-1}	0.14	0.251	1
Specific combustion heat, Q	MJ kg^{-1}	43	50	120
Emission index of water vapour, EI_{H_2O}	kg kg^{-1}	1.25	2.24	8.94
Emission index of CO_2, EI_{CO_2}	kg kg^{-1}	3.15	2.74	0
Minimum exhaust/fuel mass ratio, N_{min}	kg kg^{-1}	15.7	18.2	35.3
Ratio of EI_{H_2O}/Q relative to kerosene	1	1	1.54	2.57

Table 2. Flight conditions of a B747 burning kerosene.

Tabelle 2. Flug-Bedingungen einer B747 mit Kerosin-Treibstoff.

Parameter	Unit	Value
Pressure, p	hPa	220
Temperature, T_E	°C	−59
Relative humidity, U	%	42
True air speed, V	m s^{-1}	247
Thrust per engine, F	kN	31.1
Fuel flow rate per engine, $\dot{m}_F$	kg s^{-1}	0.58
Propulsion efficiency, $\eta = FV/(\dot{m}_F Q)$	1	0.308
Specific fuel consumption, $SFC = \dot{m}_F/F$	mg s^{-1} N^{-1}	18.7

Table 3. Contrail parameter values for various fuels.

Tabelle 3. Parameter von Kondensstreifen für verschiedene Treibstoffe.

Parameter	Unit	Kerosene	Methane	Hydrogen
G	Pa K^{-1}	1.49	2.31	3.82
T_F	K	306.7	306.7	306.7
$\dot{m}_F = FV/(Q\eta)$	kg s^{-1}	0.58	0.499	0.208
T_{LC}	°C	−50.6	−46.3	−41.2
T_{IC}	°C	−45.7	−41.8	−37.1
T_{I1}	°C	−27.9	−21.8	−14.7
T_{L1}	°C	−32.4	−25.3	−17.1
T_{IM}	°C	−39.8	−35.5	−30.4
T_{LM}	°C	−42.9	−38.3	−32.7
T_{L2}	°C	−58.0	−58.4	−58.6
T_{I2}	°C	−58.8	−58.9	−58.9
T_E	°C	−59.0	−59.0	−59.0
N_{L1}	1	1114	1022	1972
N_{LM}	1	1842	1664	3141
N_{I2}	10^5	1.27	2.35	9.78
D_{L1}	m	3.23	2.92	2.66
D_{LM}	m	4.07	3.62	3.25
D_{I2}	m	32.6	41.4	54.1
m_E	mg kg^{-1}	26.2	26.2	26.2
S_{LM}	%	78	115	157
α_{LM}	1	0.11	0.17	0.28
m_{LM}	mg kg^{-1}	278	630	1371
m_{IM}	mg kg^{-1}	409	796	1567

ture at 250 hPa was −60°C with about 20 % relative humidity. The two jet plumes on each side rotate around each other in the trailing vortex system (EHRET and OERTEL 1994) and possibly merge after some time into one contrail for each side. Based on a wing span of 60 m (note that the aircraft is seen at an angle of about 30° relative to nadir), one can measure the initial jet contrail diameters to be about 4 m, as computed.

Fig. 2 shows a photo of the contrail as observed from the DLR research aircraft Falcon about 20 km behind the B747 aircraft under conditions as given in Table 2. We observe two rather thick contrails which include the exhaust from two engines each. Obviously, the plumes got disturbed by ambient air motions causing an increase in lateral spacing between the two plumes, which we estimate to be 80–100 m, implying a diameter of 35–45 m for each contrail plume.

The final diameter D_{I2} (and the length) of dissipating contrails is the larger the higher the external humidity, see Fig. 6a. This diameter grows unlimited for ice saturation (58 % relative humidity for $T_E = 59$°C). For the observed diameter of the double jet contrails with $\sqrt{2}\ D_{I2} \cong 40$ m, Fig. 6a indicates that the ambient humidity must have been close to 45 %, which supports the measured value. Similar studies were performed by AUFM KAMPE (1942) who deduced that the relative humidity in the upper troposphere is close to 50 % on average based on statistics of contrail observations.

In contrast, the diameter D_{L1} of the young contrail is fairly insensitive to external humidity. For conditions as in Table 2, D_{L1} reduces by 1.5 % when the relative humidity increases from 0 to 100 %, see Fig. 6a. The diameter of the young contrail is also a weak function of ambient temperature and pressure. As shown in Fig. 6b, D_{L1} increases with temperature when approaching the threshold temperature T_{LC}, where the curves end. Ambient humidity affects these

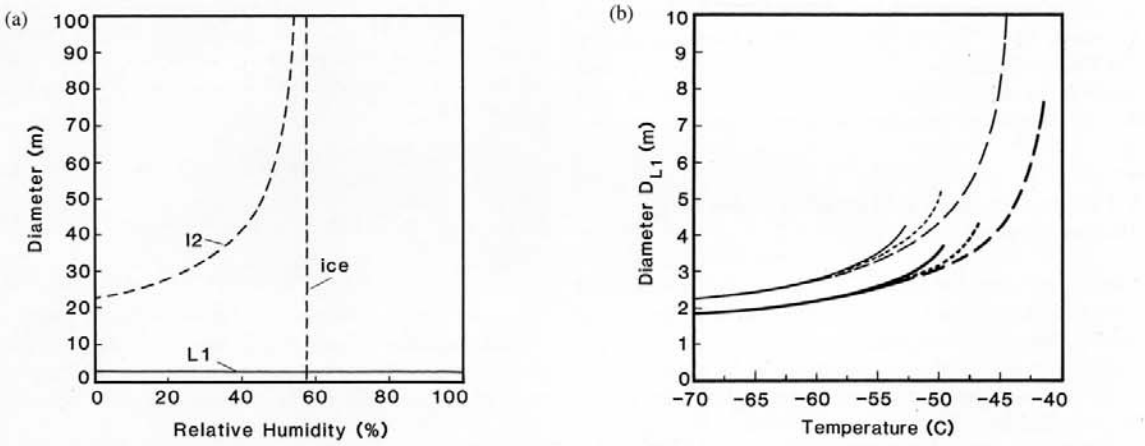

Fig. 6 (a). Contrail diameter at liquid saturation (L1) and at ice evaporation (I2) versus relative humidity under conditions as given in Table 2. For I2, $\sqrt{2}\ D_{I2}$ is plotted as appropriate for a contrail formed by two jet engines. The vertical dashed line indicates ice saturation humidity. (b) Diameter D_{L1} versus temperature T_E for conditions as in Table 2 (220 hPa, upper, thin curves) and at 300 hPa (lower, thick curves), for three ambient humidity conditions: totally dry (full), ice saturation (short-dashed), and water saturation (long-dashed).

Abb. 6 (a). Durchmesser des Kondensstreifens bei Wassersättigung (L1) und bei Eisverdunstung (I2) als Funktion der relativen Feuchte für Bedingungen wie in Tabelle 2. Für I2 wurde $\sqrt{2}\ D_{I2}$ dargestellt, entsprechend dem Durchmesser eines Kondensstreifens aus zwei Strahltriebwerken. Die vertikale strichlierte Linie kennzeichnet die Eissättigungsfeuchte. (b) Durchmesser D_{L1} als Funktion der Temperatur T_E für Parameter wie in Tabelle 2 (220 hPa, obere, dünne Kurvenschar) und für 300 hPa (untere, dicke Kurvenschar), für verschiedene Umgebungsfeuchten: völlig trocken (volle Kurven), Eissättigung (kurz gestrichelt) und Wassersättigung (lang gestrichelt).

threshold temperatures but otherwise have little effect on D_{L1}. For given jet plume mixing rates, the plume diameter is a certain function of distance behind the engines. Hence, the small sensitivity of D_{L1} to ambient conditions explains why most contrails start in a narrow range of distances behind a given aircraft. Moreover, we see from Fig. 6b that the diameter of the young contrail decreases with pressure. Hence, lower flying aircraft produce contrails which are geometrically thicker and start at slightly longer distance behind the aircraft.

However, only part of the emitted water vapour remains contained in the vortex. Other parts may get detrained from the vortex and form a curtain of emissions in the wake of the sinking vortex pair (SCORER and DAVENPORT 1970, CIAP 1975). Moreover, photos (R. ALHEIT, personal communication 1995) indicate that the outer jet contrails of a four-engine aircraft are closer to the vortex axes and persist longer than the inner ones which rotate with the outer edge of the vortices and evaporate by mixing earlier.

As a further test we consider the case of a B747-200 described in SCHUMANN (1994), which flew at 12 UTC 9 April 1991 at 10.7 km altitude (238 hPa), at a speed of 225 m s^{-1}, 100 km north of Munich, and for which the diameters of the two visible contrails have been measured in the vortex regime by lidar methods to be less than 15.5 m at a distance of 5 km after the aircraft. The meteorological sounding of Munich at that time and altitude indicates a temperature of $T_E = -63°C$ with dew point temperature of $-74°C$, i.e. relative humidity of 21 %. Further north (Meiningen, 160 km north of the aircraft) the air was more humid so that these data give the minimum plume diameters. Taking η and $\dot{m}_F$ as in Table 2, one computes $D_{l2} = 29$ m for a single jet contrail. The diameter is not much smaller for zero ambient humidity, $D_{l2} = 23$ m, and depends only weakly on η. Obviously, the computed diameter exceeds the measured value. More than one half of the water emitted must have been lost from the vortex by mixing with ambient dry air.

5. Changes in threshold conditions for large plume velocities

The theory given in section 3 accounts for the reduced amount of heat available in the young contrail due to the kinetic energy of the trailing vortex system induced by the aircraft, but ignores the kinetic energy of the plumes in the early jet phase. Hence, it applies to stagnant plumes. In this chapter the effect of non-stagnant plumes is determined.

The exhaust gases leave the engine exit plane with a large jet velocity V_j relative to ambient air. Thus the gases carry energy in form of enthalpy and kinetic energy, both resulting from the combustion energy. The kinetic energy gets gradually converted into enthalpy by turbulent dissipation when the exhaust gases mix with ambient air. Therefore, the actual temperature in the plume is lower than to be expected for a stagnant plume. Near the engine exit the exhaust gases have typically a speed V_j of 200 m s^{-1} relative to ambient air, which causes a temperature difference of $V_j^2/(2c_p)$ of order 20 K. Hence, one may ask whether the cooler, non-stagnant plume reaches saturation earlier and causes a notable increase in the threshold temperature of contrail formation.

The combustion heat leaves the engine exit in form of total specific enthalpy $h_t = h + (1/2)V_j^2$, which satisfies the same mixing laws as water mass and momentum within the well-mixed plume cross-section A,

$$N\Delta h_t = Q(1-\eta), \quad h_t = h + \frac{1}{2}V_j^2, \tag{19}$$

$$N\Delta m = EI_{H_2O}, \quad NV_j = F/\dot{m}_F, \quad N = \rho AV/\dot{m}_F. \tag{20}$$

After elimination of N and V_j from these equations, and by relating $\Delta h = c_p\Delta T$ and $\Delta e = \Delta mp/\varepsilon$, one obtains the increase in plume water partial pressure as a function of temperature increase. The result describes a mixing curve which is no longer a straight line but a parabola

$$\Delta T = \frac{\Delta e}{G} - \frac{(\Delta e)^2}{2T_F G^2}, \tag{21}$$

or an inverted parobola

$$\Delta e = \Phi(\Delta T) = G\left\{\Delta T + T_F(1 - \Delta T/T_F - [1 - 2\Delta T/T_F]^{1/2})\right\}, \tag{22}$$

depending on the two parameters G, see Eq. (8), and

$$T_F = \frac{[Q(1-\eta)\dot{m}_F]^2}{c_p F^2} = \frac{(1-\eta)^2}{\eta^2}\frac{V^2}{c_p}. \tag{23}$$

The gradient of this curve is

$$G_{eff} = d(\Delta e)/d(\Delta T) = G\left\{1 - 2\Delta T/T_F\right\}^{-1/2} = G_{eff}(\Delta T). \tag{24}$$

Obviously, the gradient becomes infinite for $\Delta T = T_F/2$, at which point the total enthalpy is split equally in internal and kinetic energy. Hence, the results are applicable only for dilution factors $N > Q(1-\eta)/(c_pT_F)$. This limit is typically of order 100 and corresponds to the dilution near the exit of jet engines. For liquid saturation, the critical conditions now follow from

$$\frac{de_L(T_{LM})}{dT} = G_{eff}(T_{LM} - T_{LC}), \tag{25}$$

$$e_L(T_{LM}) - Ue_L(T_{LC}) = \Phi(T_{LM} - T_{LC}), \tag{26}$$

$$e_L(T_{L1,L2}) - Ue_L(T_E) = \Phi(T_{L1,L2} - T_E). \tag{27}$$

For non-stagnant plumes, the value of T_{LM} depends on relative humidity of ambient air. Solutions are to be computed using a Newton iteration with the same initial guesses as given in Appendix 2. The ice saturation case follows by analogy.

As a consequence, we obtain slightly lower temperatures for the various points as indicated in Fig. 7. The impact of non-stagnant plumes ist the larger the larger $\Delta T/T_F$. For cruising aircraft with modern jet engines, the specific fuel consumption $\dot{m}_F/F$ is typically of the order $\dot{m}_F/F \cong 19 \pm 2$ mg N^{-1} s^{-1} and $\eta \cong 0.3$. For such aircraft, $T_F \cong 330$ K. When applied to the fuels specified in Table 1 and the aircraft conditions given in Table 2, the results for non-stagnant and stagnant plumes differ only a little, see Table 4. The largest differences occur in the very young contrail. The tempera-

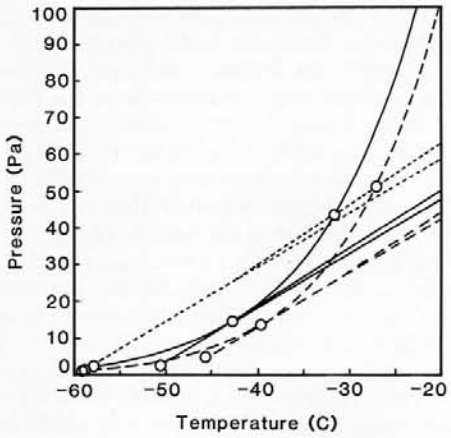

Fig. 7. As Fig. 3, according to the revised analysis, including the gradual conversion of kinetic energy into heat during mixing of the plumes with the environment. The straight mixing lines are for stagnant, the curved mixing lines with points for non-stagnant plumes.

Abb. 7. Wie Abb. 3, aber für die überarbeitete Analyse mit allmählicher Umwandlung von kinetischer Energie der Abgasfahne durch Mischung mit der Umgebung in Wärme. Die geraden Mischungskurven gelten für stagnierende Abgasfahnen, die gekrümmten mit Punkten für nicht stagnierende Abgasstrahlen.

ture T_{II} is 1 K warmer than for the stagnant plume. However the critical temperature T_{LC} and the later plume stages are affected very little by plume kinetic energy. Obviously, the velocity of the jet has got reduced considerably before reaching point I1, see Table 4. For a jet velocity of 50 m s^{-1} at I1, we expect, in fact, only a temperature change of order 1.2 K. The impact on the critical temperatures is even smaller because of the slope of the saturation curve with T. Larger differences occur for smaller aircraft speeds, see Table 4, and larger propulsion efficiencies. For the ATTAS flight observed by BUSEN and SCHUMANN (1995), with rather low propulsion efficiency of 0.14, the threshold temperature changes by only 0.1 K when comparing stagnant and non-stagnant plumes. Hence, we find that the conversion of kinetic energy of the jet into heat may be neglected in practice, except for the very young plume and for low-speed aircraft with high propulsion efficiency.

Table 4. Temperature difference between non-stagnant and stagnant plumes and jet velocity for various fuels and flight velocities.

Tabelle 4. Temperatur-Differenz zwischen stagnierenden und nicht stagnierenden Abgasfahnen und Strahlgeschwindigkeit bei verschiedenen Treibstoffen und Fluggeschwindigkeiten.

Velocity V	Parameter	Unit	Kerosene	Methane	Hydrogen
242 m s^{-1}	δT_{LC}	K	0.123	0.135	0.151
242 m s^{-1}	δT_{II}	K	0.786	0.966	1.206
242 m s^{-1}	$V_{j,II}$	m s^{-1}	56.3	67.3	80.2
160 m s^{-1}	δT_{LC}	K	0.183	0.202	0.227
160 m s^{-1}	δT_{II}	K	1.527	2.061	2.976
160 m s^{-1}	$V_{j,II}$	m s^{-1}	86.9	103.9	123.8

6. Particle properties and open questions

As we have seen, the formation of contrails depends critically on the phase of the particles. Moreover, the phase, the size and the number of the particles is important for visibility, time required to evaporate the contrail particles when diluted into subsaturated air, radiative impact on the atmosphere, possibly heterogeneous chemistry at particle surfaces, and sedimentation of the particles. Sedimentation may lead to effectively drying the upper troposphere by aviation and trigger precipitation from supercooled water clouds below the contrails (KNOLLENBERG 1972). In particular, sedimentation is important in controlling the life time of persistent contrails.

In order to sediment, the particles must grow large enough. The terminal fall speed of particles exceeds 0.1 m s^{-1}, for particles larger than 40 µm in diameter (PRUPPACHER and KLETT 1980, p. 324). These appear to be typical values, causing fall times of the order of 2000 s for 200 m thick persistent contrails. When the aircraft emits many freezing particles in frost-saturated air, then the growth of particles is limited by the amount of water available in the ambient air and not by the engine emissions. The available water depends strongly on relative humidity and temperature (GIERENS 1996). For illustration we consider a four-engine aircraft flying under conditions as in Table 2 but with near 100 % relative liquid humidity (slightly smaller values might be more realistic), forming a persistent contrail. For an assumed emission index of ice forming particles, $EI_{part} = 10^{13}$ kg^{-1}, the contrail has to spread B = 1.5 km laterally and H = 200 m vertically before the particles meet sufficient water vapour to grow to a diameter of d = 40 µm. Here, B is computed from

$$B = \frac{EI_{part} 4 \dot{m}_F (\pi/6) d^3 \rho_L}{V \rho_{air} H \, m_L}, \qquad (28)$$

with $m_L = \varepsilon(e_L - e_I)/p \cong 26$ mg kg^{-1}, and $\rho_L \cong 900$ kg m^{-3}. Such a contrail would have an optical thickness, see Appendix 3, of 0.15, a reasonable value (KÄSTNER et al. 1993), 300 particles per litre (compare GAYET et al. 1996), and the condensed particles would contain 240 times the amount of water emitted from the engines (compare KNOLLENBERG 1972). Particles may grow more quickly at the edge of the contrail where the ice particles find more water vapour (GIERENS 1996). However, these simple computations are sufficiently consistent with observations to indicate that persistent contrails are to be understood this way. Obviously, the dimensions and the life-time of persistent contrails depend strongly on the emission index for particles which can grow to large ice particles. Estimates of the ice particle emission index vary by several orders of magnitude (PITCHFORD et al. 1991, FAHEY et al. 1995, SCHUMANN et al. 1996).

Often even the phase of particles is uncertain. Since this is an important question, we recall related arguments and research, some with long history. If contrails form without freezing they should evaporate earlier than with freezing. In fact, for threshold conditions and short-lived contrails,

liquid saturation is reached only for a very short segment along the plume, but contrails are always several hundred metres long. Hence, at least some of the liquid particles freeze before all liquid water droplets evaporate. If the particles form directly by freezing when reaching saturation over ice, then the threshold temperature should be definitely 4 to 5 K higher than actually observed. This suggests that the particles form essentially on condensation nuclei when exceeding liquid saturation. The question is, do all particles freeze and how long does that take?

Because of the similarity between contrail and fog near the surface, one may consider the properties of particles in ice-fog at low temperatures (PRUPPACHER and KLETT 1980, p. 44). THUMAN and ROBINSON (1954) observed fog particles forming from steam at low temperatures at the surface in Alaska at temperatures below –20°C. Particles collected on glass slides were composed of hexagonal plates, prismatic columns, and so-called droxtals, i.e. near-spherical solid particles with rudimentary crystal faces. The relative number of droxtals increased rapidly with decreasing temperature, and below –38°C accounted for over 90 % of the observed particles. Intense scintillation was observed in a light beam but mainly from the crystals, less from the droxtals. The droxtals had mean diameters of order 10 µm, slightly increasing with temperature. A small diameter corona (i.e. ring visible around the sun or moon behind thin droplet clouds, due to diffraction and refraction of light at droplets, coloured when the particles have about the same diameter) was observed as being typical for droplets, but attempts to seed the fog with silver iodide and dry ice failed to cause any visible change and glaze ice did not form on exposed surfaces. Hence its was concluded that the particles were ice rather than supercooled water. MURCRAY (1970) reported related studies where 80 % of crystals collected near an airport runway had a diameter near 4 µm with the shape of droxtals. Some of the droxtals emitted jets of liquid while freezing from outside in (MURCRAY 1970) but ice multiplication possible from such effects have not been identified (KNOLLENBERG 1972).

On the other hand, PILIÉ and JIUSTO (1958) performed a laboratory study of contrails by burning aircraft fuels at pressures between 1000 and 300 hPa and at temperatures between ambient and –53°C. The observations showed no light scintillation from crystals, evaporation at relative humidity above ice saturation, round particles, and small visibility as computed for given water content. It was concluded that the initial phase of condensed moisture is liquid and often stayed liquid throughout the experimental conditions.

WEICKMANN (1945, 1949) collected particles in contrails at altitudes between 8 and 9 km at temperatures near –40°C with a small pad coated with "Zaponlack" and took microphotographs. Most of the particles were very small (order 1 µm), difficult to catch on the pad and to resolve with the photos. Sometimes, he found particles of 100 µm length having the form of hollow prisms, which seem to form preferentially at low temperatures with high ice supersaturation. Similar studies have been performed recently by STRAUSS (1994) with a formvar-chloroform coated impactor during flights in contrails and natural cirrus clouds. He was able to identify particles larger than 3 µm in diameter. The smallest particles visible were similar to the droxtals found by THUMAN and ROBINSON (1954) and possibly similar to those seen by PILIÉ and JIUSTO (1958). STRAUSS found that contrails which are one minute old contain typically a factor of three more particles than natural cirrus. The particles had diameters in the range 3 to 20 µm and the shape of ice crystals. In older contrails, particles became more similar to those in natural cirrus. In situ measurements (KNOLLENBERG 1972) with an optical-array particle spectrometer in persistent contrails, having four order of magnitude more water content than emitted from the aircraft, resulted in mean particle diameters of the order 0.5 mm, clearly ice crystals. Recently, BAUMGARDNER and COOPER (1994) and GAYET et al. (1996) used similar methods suited for particles of the order 1 µm and larger, and found many small particles in contrails, which were considered to be ice particles.

Also remote sensing data (BETANCOR and GRASSL 1993) indicate contrails containing more but smaller crystals than natural cirrus clouds (order 5 µm compared to 100 µm). Particles sedimenting from contrails were observed by radar (KONRAD and HOWARD 1974) and lidar (SCHUMANN and WENDLING 1990, SCHUMANN 1994), including polarization measurements (FREUDENTHALER et al. 1994), indicating quickly growing ice particles. SASSEN et al. (1985) measured the depolarization from particles in cirrus clouds. They found very small depolarization in one example at the lower edge of a natural cirrus cloud at 8.6 km altitude. In the same cloud, at temperatures between –35 and –36°C, they measured a particle density of 25–35 L^{-1} with mean diameters of 5 µm, which they classified as being liquid. However, one may ask whether frozen droxtals cause the same low depolarization.

Halo observations or mock suns (parhelion) (WEICKMANN 1919; SCHMAUSS 1919; HANCOCK 1943; BOERNER 1943; AUFM KAMPE 1943; WEICKMANN 1945, 1949; KÜTTNER 1946) indicate random or vertically oriented hexagonal ice crystals. The observations seem to refer to aged and persistent contrails, sometimes having formed large cirrus decks. DOBSON (1941, unpublished) referred to corona observations in contrails as an indication for droplets. SASSEN (1979) showed photos of a contrail with one and even part of a second corona ring which forms by diffraction of solar light at spherical and monodispersed particles as a function of wavelength and particle diameter, see also GREENLER (1980). From this iridescence phenomenon, SASSEN (1979) deduced that the particle diameters increased from 2 to 3 µm diameter within 200–400 m distance behind the aircraft. Since the particles must have been round, it was suggested that this indicates droplets in the contrails. However, monodispersed near-spherical ice-crystals may induce the same optical effect (GREENLER 1980, SASSEN et al. 1989). Hence there is no doubt that ice particles of diameters between 1 and 20 µm are formed, but it is still not clear at which time scales.

Many observations have shown that contrails form quickly after the engines, typically within a distance of 10–30 m (AUFM KAMPE 1943, BUSEN and SCHUMANN 1995, SCHUMANN et al. 1996). Fig. 1 shows that contrails form before the jet plumes reach the aircraft tail. KÄRCHER et al. (1995) computed the nucleation and growth of particles forming from homogeneous nucleation of sulphuric acid with water vapour. They found that under threshold conditions with typical amounts of fuel sulphur content such particles do not grow quick enough to freeze and then grow to visible particles within the time scales where contrails are observed to form. The experiments of SCHUMANN et al. (1996) indicate that particles form at least partly by condensation on soot particles. It is conceivable that visible ice particles form slightly below liquid water saturation when the temperature is below –35°C (PRUPPACHER and KLETT 1980, p. 245, HEYMSFIELD and SABIN 1989, SASSEN and DODD 1989), in particular when sulphuric acid and soot particles are present (ZHAO and TURCO 1995, B. KÄRCHER, personal communication 1995). Hence, emissions of sulphur and soot from aviation may enhance early contrail formation but the details remain unclear.

It should be noted that engines burning liquid hydrogen will be essentially free of soot and sulphur emissions (except from burning air with sulphur containing molecules). It can be expected that such engines emit far less particles than engines burning kerosene. It appears likely that a smaller number of particles emitted will lead to larger droplets and ice particles. Such a contrail would exhibit a smaller optical thickness in spite of the larger water content, see Appendix 3. Moreover, the particles would sediment earlier than for a larger initial particle density. This suggests that aircraft burning liquid hydrogen will cause persistent contrails which are of shorter life-time, and possibly less climate impact than aircraft burning kerosene. Liquid methane might be burnt sootless but may contain sulphur containing gases when originating from natural gas sources.

Many other aspects of contrail formation and impact on climate exist which cannot be covered in this article. These include the jet and vortex dynamics, the vortex brake up and later diffusion regime of the contrail plume (DOWNIE and SILVERMAN 1957; SCORER and DAVENPORT 1970; CIAP 1975; SCHILLING 1992; MIAKE-LYE et al. 1993; KÄRCHER and FABIAN 1994; KÄRCHER 1994; EHRET and OERTEL 1994; SCHUMANN et al. 1995, 1996; GIERENS 1996), see also SCHUMANN and WURZEL (1994) and SCHUMANN (1995). Details of mixing are important in the jet phase, the vortex phase and the dispersion phase (CIAP 1975): Mixing in the jet phase determines the distance behind the engines and the dilution necessary for reaching saturation. Non-similar mixing of the core jet with the bypass jet may cause local saturation earlier than predicted for complete mixing of both jets. The stability of the trailing wing vortices controls the length of short-lived contrails. The dispersion in the late phase controls the width of persistent contrails. Radiation and latent heat release seem to have small impact on the contrail dynamics in the first half hour but upward motion may enhance contrails considerably (GIERENS 1996).

Other open topics of importance are the objective identification of contrails from satellite data (SCORER 1986, CARLETON and LAMB 1986, LEE 1989, ROLL 1990, SCHUMANN and WENDLING 1990, ENGELSTAD et al. 1992, KÄSTNER et al. 1993, BETANCOR and GRASSL 1993; BAKAN et al. 1994), the relation of contrail occurrence to the meteorological conditions, and development of suitable forecast and simulation rules (GOLDIE and HORROCKS 1941–1942, unpublished; AWS 1953, 1956, 1981; JIUSTO and PILIÉ 1964; DETWILER and PRATT 1984; CARLETON and LAMB 1986; SCHUMANN and WENDLING 1990; BJORNSON 1992; PETERS 1993; BAKAN et al. 1994), chemical effects (WMO 1995), and the climatic impact of contrails (REINKING 1968, KUHN 1970, GRASSL 1990, LIOU et al. 1990, BETANCOR and GRASSL 1993). The list of references is not complete.

The water vapour emitted from aircraft impacts the climate in many ways, including reduced solar radiation at the ground, the greenhouse effect of enhanced water vapour, narrow short-lived contrails, and extended persistent contrails. Variations in solar radiation, significant compared to natural variability, have not been conclusively identified (JACOBS 1971, CHANGNON 1981, SEAVER and LEE 1987, HAUPT and ROTTER 1991, LIEPERT et al. 1994). The pure greenhouse effect of the water vapour emitted from aircraft appears to be small at altitudes of subsonic aircraft (RIND and LONERGAN 1995, FORTUIN et al. 1995, PONATER et al. 1996). As noted before, contrails may even reduce the water vapour content at flight levels by sedimentation. However, significant radiative changes and climatic impact by persistent contrails cannot be excluded (FORTUIN et al. 1995, PONATER et al. 1996). More definite statements require progress with respect to analysis and simulation of humidity, particle formation, and frequency and radiative properties of contrails.

7. Conclusions

The topic of contrail research is now more than 75 years old. Although many questions are still open, the literature review has revealed some interesting, partly overlooked results. The theory of contrail formation was developed around 1940 simultaneously at several places. The basic thermodynamics was most clearly explained by SCHMIDT (1941). This theory, as also given in APPLEMAN (1953), has been reexamined in this paper in order to clarify the basic assumptions involved and to show the impact of the fact that part of the combustion heat is converted to kinetic energy causing lower threshold temperatures for contrail formation. The algorithms required to evaluate the Schmidt/Appleman criterion have been described in detail, and approximative equations have been provided. The kinetic energy of the young exhaust plumes has only a minor effect on the threshold conditions. It leaves previous interpretations of the ATTAS experiment (BUSEN and SCHUMANN 1995) unchanged. Analysis of measured B747 cases show that measured contrail diameters fit the computations roughly. However, part of the water mass emitted from the

aircraft gets lost from the vortex system containing the contrail. An increase in propulsion efficiency by 10 % extends the region where contrails may form 280 m downwards and even more to higher altitudes. Many open questions have been identified. The most important ones concern the emission index of ice-forming particles per fuel mass, the frequency of frost-saturated air conditions supporting persistent contrails, and the properties and climatic impact of such contrails. Also, the threshold temperature for contrail formation may depend on details of turbulent mixing in the early jet phase when the engine emits moisture and heat with different initial profiles, as is the case for modern bypass engines.

The theory has been applied to a typical large aircraft with standard kerosene fuel and with the potential alternatives liquid methane and hydrogen. Engines burning liquid hydrogen emit 2.6 times more water vapour than kerosene for the same amount of combustion heat. Hence, contrails form behind liquid hydrogen-propelled aircraft at typically 10 K higher temperatures, i.e. at lower tropospheric and higher stratospheric altitudes and may grow to larger diameter before evaporating. However, this does not necessarily mean that hydrogen-propelled aircraft cause stronger impact on climate, since the water vapour emissions from subsonic aviation appears to be far too small to cause appreciable greenhouse effects when remaining in the gas phase and the contrails formed from such liquid hydrogen have particle properties, optical thicknesses and life-times different from kerosene fuels and their climatic impact cannot be easily assessed, therefore. The properties of contrails caused by burning liquid methane are between those resulting from kerosene and hydrogen fuels.

Appendix 1: Emission indices of aviation fuels

Aviation fuels contain carbon and hydrogen besides some sulphur and small amounts of minor constituents (CRC 1983, GOODGER and VERE 1985, ODGERS and KRETSCHMER 1986). The sulphur content of Jet-A1 fuel, a standard aviation kerosene, is restricted to maximum values of 0.3 % by mass or 3000 ppm (ASTM 1994); in practice, fuels have 400–550 ppm sulphur mass content on average, with one third of the fuels having less than 100 ppm sulphur content (P. BROWN, Kuwait Petrol, UK, unpublished 1995), see also SCHUMANN (1994), and BUSEN and SCHUMANN (1995). Aviation fuel specifications do not fix the hydrogen content. The hydrogen mass content m_H varies typically between 13.8 and 14 % (L. G. MILNE, Kuwait Petroleum, UK, personal communication 1995), but samples have been found with values between 13 and 14.5 %.

For 100 % combustion (neglecting unburnt hydrocarbons, carbon monoxide, soot, and other minor emissions), the exhaust contains EI_{H_2O} mass units of carbon dioxide per unit fuel mass, with

$$EI_{H_2O} = \frac{m_H M_{H_2O}}{2M_H}, \quad EI_{CO_2} = \frac{m_C M_{CO_2}}{M_C}, \tag{29}$$

where M_H = 1.008, M_{H_2O} = 18.016, M_C = 12.011, and M_{CO_2} = 44.011 are the molar masses of hydrogen, water, carbon, and carbon dioxide. Burning one mass unit of fuel with (N – 1) mass units of air results in N mass units of exhaust. Stoichiometric combustion requires one molecule of oxygen per carbon atom and ¼ molecule of oxygen per hydrogen atom in the fuel. Hence, complete combustion with air containing a mass fraction $m_{O_2} \equiv 0.2314$ of oxygen (M_{O_2} = 32) requires $N > N_{min}$, with

$$N_{min} = \frac{m_C/M_C + (1/4)m_H/M_H}{m_{O_2}/M_{O_2}} + 1. \tag{30}$$

Jet engines burn with an air excess so that N is typically of the order 50–70 at the exist of the core engine. The emission indices and minimum dilution factors are listed for three fuels in Table 1 (for zero sulphur content).

Table 1 contains also the specific heat of combustion Q, which is the so-called net or lower heat value, i.e. the heat resulting from burning liquid fuels at a standard temperature (15°C for Jet-A1, ASTM 1994) and forming gaseous exhaust products without latent heat release from condensing water vapour in the exhaust. The specification of Jet-A1 requires$Q \geq 42.8$ MJ kg^{-1}, maximum values are 43.8 MJ kg^{-1} (CRC 1983). The other Q values are from WINTER (1990).

Appendix 2: Estimates on critical temperatures

Approximative relations are needed to estimate the critical temperatures as defined in section 3. The temperature T_{LM} is determined from Eq. (10) by a Newton iteration. As a first guess and good approximation one may use

$$T_{LM} = -46.46 + 9.43 \ln(G - 0.053) + 0.720[\ln(G - 0.053)]^2, \tag{31}$$

for T_{LM} in units of °C and G in units of Pa K^{-1}. This least-square fit gives a maximum error of 0.056°C for 0.24 Pa K^{-1} ≤ G < 23 Pa K^{-1}, i.e. for –60°C ≤ T_{LM} ≤ –10°C. Similarly, T_{IM} is approximated by

$$T_{IM} = -43.36 + 9.08 \ln(G - 0.02) + 0.49 [\ln(G - 0.02)]^2, \tag{32}$$

with maximum error of 0.036°C for 0.15 Pa K^{-1} ≤ G < 23 Pa K^{-1}.

For U = 0 and U = 1, T_{LC} and T_{IC} follow explicitly from Eqs. (11) and (12). Otherwise, approximate values are obtained from a Taylor expansion around point LM giving

$$T_{LC} = T_{LM} - x, \; x = -A + (A^2 + 2B)^{1/2}, \tag{33}$$

with

$$A = \frac{(1 - U)G}{U^2 e''_L(T_{LM})}, \quad B = \frac{e_L(T_{LM}) - e_E}{U^2 e''_L(T_{LM})}, \quad e_E = U e_L(T_{LM}), \tag{34}$$

and analogous equations for T_{IC}. If $T_E < T_{LC}$, then the solutions for points L1 and L2 exist. First guesses are

$$T_{L1,L2} = T_{LM} \pm x, \quad x^2 = 2\{e_E - e_L(T_{LM}) + G(T_{LM} - T_E)\}/e''_L(T_{LM}). \tag{35}$$

Values for T_{I1} and T_{I2} are obtained likewise by replacing e_L by e_I. However, for U being defined as relative humidity for liquid saturation, the ambient partial pressure e_E is still given by Ue_L. The saturation pressures for liquid and ice saturation are computed from relations as given in SONNTAG (1994) for the temperature range down to – 100°C. The first and second derivatives, $e'_L = de_L/dT$, $e''_L = d^2e_L/dT^2$, are computed numerically from these relations.

Appendix 3: Visibility of contrails

A condensation trail is visible by virtue of the light scattered by the trail constituents in the direction to the observer. The luminance of the trail depends on the light-scattering properties of the particles in the trail and the intensity and direction of the incident light. The contrail becomes visible to a human observer if the luminance contrast exceeds a certain threshold value. This requires an optical thickness τ of at least 0.02. The optical thickness $\tau = D(\pi/4)d^2Q_{ext}n$ depends on the number density of particles n, the diameter of the particles d, the geometrical thickness of the contrail D (depending on the viewing angle) and the extinction efficiency Q_{ext} (VAN DE HULST 1957). The latter increases nonlinearly from zero with d for d less than the wavelength λ of light (near 0.55 µm), oscillates when $d/\lambda = O(1)$ and approaches 2 for $d/\lambda > 1$. For given or estimated particle size, the number density follows from $n = m_L\rho 6/(\pi d^3\rho_L)$, depending on the mass fraction m_L of liquid (or ice) water available, and the densities of air ρ and particles ρ_L. As a consequence,

$$\tau = (3/2)(D/d)Q_{ext}m_L(\rho/\rho_L). \qquad (36)$$

Visibility also depends strongly on the viewing angle (PILIÉ and JIUSTO 1958, KNOLLENBERG 1972). Because of the preferentially foreward scattering of light by small particles, contrails are best visible when viewed at a small angle against the sun.

DOBSON (1941, unpublished) estimated the visibility and concluded that water droplets of 2 µm diameter are sufficient for a contrail of 50 m thickness to become visible for a liquid water content of 0.1 g m^{-3}. APPLEMAN (1953, 1957) required 0.004 g m^{-3} for a faint trail and 0.01 g m^{-3} for a distinct trail. For unfavourite viewing conditions, larger water contents of the order 0.1 g m^{-3} are required (JIUSTO and PILIÉ 1964). Hence, visible contrails form at slightly smaller threshold temperatures than computed for zero water content, in particular at low pressures, with small differences between water and ice saturation (APPLEMAN 1953). However, precise threshold values cannot be given without knowing the particle spectrum and the viewing conditions. For constant extinction efficiency $Q_{ext} = 2$, i.e. particle diameters $d > 2$ µm, the optical thickness of the B747 burning kerosene as specified in Table 2 causes jet plumes with a maximum of $\tau \cong 0.4$ for $d = 2$ µm, and τ decreases with d^{-1} for larger particles. For persistent contrails, optical thicknesses of order one have been measured (SCHUMANN and WENDLING 1990, KÄSTNER et al. 1993).

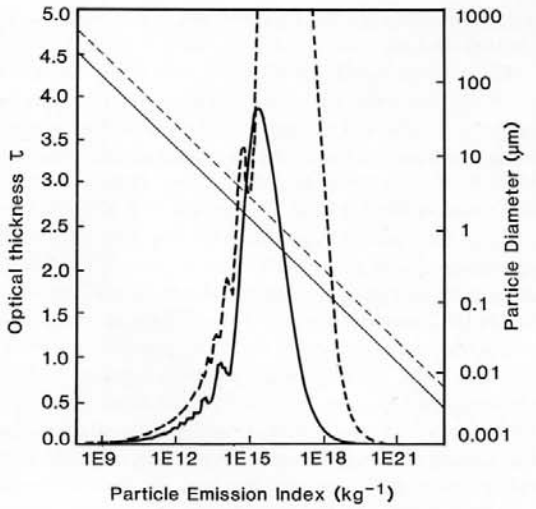

Fig. 8. Optical thickness τ versus particle emission index EI_{part} for ice particles (notation 1E9 for 10^9) formed from kerosene (full thick curve, maximum: 3.84) and liquid hydrogen (dashed thick curve, maximum: 13.7, not plotted) fuels, and corresponding particle diameters (thin lines). Parameters as in Tables 2 and 3 for point LM.

Abb. 8. Optische Dicke τ als Funktion des Partikel-Emissions-Index EI_{part} (1E9 steht für 10^9) für Eispartikel aus Kerosin (volle dicke Kurve) und flüssigem Wasserstoff (gestrichelte dicke Kurve) als Treibstoff und zugehörige Partikel-Durchmesser (dünne Geraden). Parameter wie in Tabellen 2 und 3 für Punkt LM.

Fig. 8 shows the optical thickness computed for a size-dependent extinction coefficient (with a Mie routine provided by K. GIERENS) versus emission index EI_{part} of ice-forming particles per unit fuel mass, assuming equal-sized and spherical ice particles of diameters d with $d^3 = m_LN/(EI_{part}\rho_L\pi/6)$. The number density of the particles is computed from $n = EI_{part}\rho/N$. The dilution factor N and the plume diameter D are taken from Table 3 for point LM. The amount of condensable water m_L has been computed without accounting for the reduction by latent heat release. We see that the optical thickness τ is small for $EI_{part} < 10^9$ kg^{-1}, grows with oscillations according to the Mie theory, reaches a maximum for $EI_{part} \cong 3\times10^{16}$ kg^{-1}, and decays again to zero for $EI_{part} > 10^{19}$ kg^{-1}. The (equilibrium) particle diameters decrease over five orders of magnitude. Estimated emission indices for kerosene engines vary between $EI_{part} \cong 10^{11}$ and 10^{15} kg^{-1} (KNOLLENBERG 1972, SCHUMANN et al. 1996), within the range of increasing visibility. The particle emission from engines burning hydrogen fuels may equal the amount of particles entering the engine with the ambient air. For a typical particle concentration of 100 cm^{-3}, an air/fuel mass flow ratio in the engine of 60, and an air density of 0.3 kg m^{-3}, the number of particles correspond to an emission index of $EI_{part} \cong 2\times10^{10}$ kg^{-1}. Such engines may emit less particles than kerosene engines and cause plumes with larger particles but smaller optical thickness, even

when accounting for the 4.5 times larger water-path available at point LM.

The contrail would be invisible also when containing very many very small particles. This is supported by the fact that proposals have been made to suppress the formation of visible contrails by the injection of chlorosulphonic acid $HClSO_3$ (ANDERSON et al. 1970), chloro-fluoro-sulphonic acid (Aviation Week & Space Techn. Vol. 129, Nov. 28, 1988, p. 21), or detergents formed from water solutions containing monohydric or polyhydric alcohols, possibly in combination with inorganic nucleating salts such as silver iodide (SINGH 1992) into the hot jet exhaust. These additives either form artificial condensation nuclei or promote nucleation by reducing the surface stress of droplets forming. Chlorosulphonic acid is decomposed by heat from the engine exhaust into hydrogen chloride and sulphur trioxid. Sulphur trioxid is a hygroscopic material that takes up water readily and acts to nucleate the trail. When the contrail particles stay smaller than an order of 0.5 μm, the resultant particles appear as blue haze with low contrast against the background (SINGH 1992). From Fig. 8, we expect optical thicknesses below 0.02 when the particles stay smaller than 0.06 μm, and this requires more than 10^{19} kg^{-1} ice-forming particles per fuel mass for the kerosene case. Visibility could also be avoided by using fuels with low hydrogen contents. In fact, carbon sulfide CS_2 has been shown to be applicable as engine fuel in altitude test facilities causing a thinner fog from nucleation of sulphur trioxid with ambient humidity (HELD and DIETZ 1944, unpublished). Such fuels and additives have many undesirable properties (the acids are corrosive and the emitted particles may change cloudiness) and are certainly unsuited for aviation in general.

Acknowledgements

I thank colleagues and librarians of the Meteorological Office, Bracknell, UK, of the Scott Air Force Base, Illinois, USA, of the Royal Netherlands Meteorological Institute, De Bilt, of the Deutscher Wetterdienst, Offenbach, of the Deutsches Museum, München, and of the Deutsche Forschungsanstalt für Luft- und Raumfahrt (DLR), Oberpfaffenhofen, for providing copies of articles and informations which were not available otherwise. This work is part of the research project "Schadstoffe in der Luftfahrt", supported by the German Federal Ministry BMBF. The aircraft parameters of Table 2 correspond to observations taken within the project POLINAT, Pollution of the North Atlantic Flight Traffic Corridor, funded by the European Commission.

References

Alheit, R., 1995: Box-Modellrechnungen zur Mikrophysik in Cirren eingebetteter Kondensfahnen. — Ann. Meteorol. **31**, 226.

Anderson, C. E., S. J. Birstein, B. A. Silverman, 1970: Method and apparatus for suppressing contrails. — US Patent 3,517,505.

Appleman, H., 1953: The formation of exhaust condensation trails by jet aircraft. — Bull. Amer. Meteorol. Soc. **34**, 14–20.

— 1957: Derivation of jet-aircraft contrail-formation curves. — Air Weather Service, Washington, AWS TR 105-145, pp. 46.

ASTM, 1994: Standard specification for aviation fuels, D 1655-93a. — Annual Book of ASTM Standards, 05.01. American Society for Testing and Materials, Philadelphia, PA 19103-1187, p. 555–563.

Aufm Kampe, H. J., 1942: Kondensation und Sublimation in der oberen Troposphäre. — Deutsche Luftfahrtforschung, Forschungsbericht Nr. 1491, Berlin, pp. 60 (available at Deutsches Museum Munich).

— 1943: Die Physik der Auspuffwolken hinter Flugzeugen. — Luftwissen **10**, 171–173. English in NASA-TT-F-14047 (1971).

AWS, 1953: An analysis of some contrail data. — Air Weather Service, Washington 25, D.C., AWS Techn. Report No. 105–103, pp. 13.

— 1956: Preliminary results of project Cloud Trail. — Air Weather Service, Washington 25, D.C., AWS Techn. Report No. 105–132, pp. 23.

— 1981: Forecasting aircraft condensation trails. — Air Weather Service, Scott AFB, Illinois 62225, AWS/TR-81/001, AD-A111876, pp. 21.

Bakan, S., M. Betancor, V. Gayler, H. Graßl, 1994: Contrail frequency over Europe from NOAA-satellite images. — Ann. Geophys. **12**, 962–968.

Baschin, O., 1919: Flugzeuge als Wolkenbildner und Wolkenfresser. — Deutsche Luftfahrer-Z. **6**, H. 13–14, 6.

Baumgardner,D., W. A. Cooper, 1994: Airborne measurements in jet contrails: Characterization of the microphysical properties of aircraft wakes and exhausts. — DLR-Mitt. 94-06, DLR, D-51140 Köln, 418–423.

Betancor-Gothe, M., H. Graßl, 1993: Satellite remote sensing of the optical depth and mean crystal size of thin cirrus and contrails. — Theor. Appl. Climatol. **48**, 101–113.

Bjornson, B. M., 1992: SAS Contrail formation study. — USAF Environmental Techn. Appl. Center, Scott Air Force Base, Illinois, USAFETAC/PR-92/003, AD-A254 410, pp. 44.

Boerner, H., 1943: Haloerscheinungen an Kondensfahnen. — Z. angew. Meteorol. **60**, 397.

Brewer, A. W., 1946: Condensation trails. — Weather **1**, 34–40.

Busen, R., U. Schumann, 1995: Visible contrail formation from fuels with different sulfur contents. — Geophys. Res. Lett. **22**, 1357–1360.

Carleton, A. M., P. J. Lamb, 1986: Jet contrails and cirrus clouds: A feasibility study employing high-resolution satellite imagery. — Bull. Amer. Meteorol. Soc. **67**, 301–309.

Changnon, S. A., 1981: Midwestern cloud, sunshine and temperature trends since 1901: Possible evidence for jet contrail effects. — J. Appl. Meteorol. **20**, 496–508.

Chigier, N. A., 1974: Vortexes in aircraft wakes. — Sci. Amer. **230**, March, 76–83.

CIAP, 1975: The Stratosphere perturbed by propulsion effluents. — CIAP Monogr. 3, Departm. Transport., Climatic Impact Assessment Program, Washington, D.C., DOTTST-75-53.

CRC, 1983: Handbook of Aviation Fuel Properties. — Coordinating Research Council, Soc. Automotive Engineers, Warrendale, Pennsylvania 15096, USA, pp. 112.

DeGrand, J. Q., A. M. Carleton, P. J. Lamb, 1990: A mid-season climatology of jet condensation trails from high resolution satellite data. — Proc. 7th Conf. Atmospheric Radiation, July 23–27, San Francisco, Calif., Amer. Meteorol. Soc., Boston, 309–311.

Descamps, A. M., 1945: Les traînées blanches d'avions. — Belgium, Inst. Roy. Météorol. **17**, 3–23.

Detwiler, A., R. Pratt, 1984: Clear-air seeding: Opportunities and strategies. — J. Wea. Mod. **16**, 46–60.

Dobson, G. M. B., A. W. Brewer, B. M. Cwilong, 1946: Meteorology of the lower stratosphere. — Proc. Roy. Soc. A **186**, 144–175.

Downie, C. S., B. A. Silverman, 1957: Jet aircraft condensation trails. — Chapter 19 in Campen, C. F. et al. (eds.), Handbook of Geophysics for Air Force Designers. Air Force Geophysics Lab., Hanscom AFB, Ma., AD-A955 708/3/XAD, pp. 1–9.

Ehret, T., H. Oertel, 1994: Numerical simulation of the dynamics and decay of trailing vortices including pollutants from air traffic. — DLR-Mitt. 94-06, DLR, D-51140 Köln, 268–273.

Engelstad, M., S. K. Sengupta, T. Lee, R. M. Welch, 1992: Automated detection of jet contrails using AVHRR split window. — Int. J. Rem. Sens. **13**, 1391–1412.

Ettenreich, R., 1919: Wolkenbildung über einer Feuersbrunst und an Flugzeugabgasen. — Meteorol. Z. **36**, 355–356.

Fahey, D. W., E. R. Keim, E. L. Woodbridge, R. S. Gao, K. A. Boering, B. C. Daube, S. C. Wolfsy, R. P. Lohmann, E. J. Hintsa, A. E. Dessler, C. R. Webster, R. D. May, C. A. Brock, J. C. Wilson, P. O. Wennberg, R. C. Cohen, R. C. Miake-Lye, R. C. Brown, J. M. Rodriguez, M. Loewenstein, M. H. Proffitt, R. M. Stimpfle, S. Bowen, K. R. Chan, 1995: In situ observations in aircraft exhaust plumes in the lower stratosphere at mid-latitudes. — J. Geophys. Res. **100**, 3065–3074.

Fortuin, J. P. F., R. van Dorland, W. M. F. Wauben, H. Kelder, 1995: Greenhouse effects of aircraft emissions as calculated by a radiative transfer model. — Ann. Geophys. **13**, 413–418.

Freudenthaler, V., H. Jäger, F. Homburg, 1994: Ground based mobile scanning lidar for remote sensing of contrails. — Ann. Geophys. **12**, 956–961.

Gayet, J.-F., G. Febvre, G. Brogniez, H. Chepfer, W. Renger, P. Wendling, 1996: Microphysical and optical properties of cirrus and contrails: Cloud field study on 13 October 1989. — J. Atmos. Sci., **53**, 126–138.

Gierens, K., 1996: Numerical simulations of persistent contrails. — J. Atmos. Sci., submitted.

Goodger, E., R. Vere, 1985: Aviation Fuels Technology. — MacMillan, Houndsmill, pp. 265.

Grassl, H., 1990: Possible climatic effects of contrails and additional water vapour. — Lecture Notes in Engrg., Vol. **60**, Springer, Berlin, 124–137.

Green, W., G. Swanborough, 1991: Airliners. — Bloomsbury Books, London, pp. 192.

Greenler, R., 1980: Rainbows, Halos and Glories. — Cambridge Univ. Press. p. 141–142 and 182.

Hagen, H., 1982: Fluggasturbinen und ihre Leistungen. — Braun, Karlsruhe, pp. 366.

Hancock, D. S., 1943: A mock sun in vapour-trail cloud. — Quart. J. Roy. Meteorol. Soc. **69**, 46.

Haupt, H., M. Rotter, 1991: Untersuchung der Flugzeugkondensstreifen und ihrer klimatischen Auwirkungen in Kärnten. — Wetter und Leben **43**, 173–188.

Heiërman, J. H., 1944: Vliegtuigwolken. — Hemel en Dampkring **42**, 101–109.

Heymsfield, A. J., R. M. Sabin, 1989: Cirrus crystal nucleation by homogeneous freezing of solution droplets. — J. Atmos. Sci. **46**, 2252–2264.

Höhndorf, F., 1939: Eiswolken-Erzeugung in größeren Höhen durch Flugzeuge. — Deutsche Luftfahrtforschung, Berlin, FB 1134, pp. 13.

Iribarne, J. V., W. L. Godson, 1981: Atmospheric Thermodynamics. — Reidel, Dordrecht, pp. 259.

Jacobs, J. D., 1971: Aircraft contrail effects on the surface radiation budget in an Arctic region. — Bull. Amer. Meteorol. Soc. **52**, 1101–1102.

Jiusto, J. E., R. J. Pilié, 1964: Contrails forecasting. — Cornell Aeron. Lab., CAL-Rep. No. VC-1660-P-3, AD 692 119.

Kärcher, B., 1994: Transport of exhaust products in the near trail of a jet engine under atmospheric conditions. — J. Geophys. Res. **99**, 14509–14517.

Kärcher, B., P. Fabian, 1994: Dynamics of aircraft exhaust plumes in the jet-regime. — Ann. Geophys. **12**, 911–919.

Kärcher, B., Th. Peter, R. Ottmann, 1995: Contrail formation: Homogeneous nucleation of H_2SO_4/H_2O droplets. — Geophys. Res. Lett. **22**, 1501–1504.

Kästner, M., K. T. Kriebel, R. Meerkötter, W. Renger, G. H. Ruppersberg, P. Wendling, 1993: Comparison of cirrus height and optical depth derived from satellite and aircraft measurements. — Mon. Wea. Rev. **121**, 2708–2717.

Kelly, R. D., G. Vali, 1991: An experimental study of the production of ice crystals by a twin-turboprop aircraft. — J. Appl. Meteorol. **30**, 217–226.

Knollenberg, R. G., 1972: Measurements of the growth of the ice budget in a persisting contrail. — J. Atmos. Sci. **29**, 1367–1374.

Köhler, H., 1936: The nucleus in and the growth of hygroscopic droplets. — Trans. Faraday Soc. **32**, 1152–1161.

Konrad, T. G., J. C. Howard, 1974: Multiple contrail streamers observed by radar. — J. Appl. Meteorol. **13**, 563–572.

Kramer, M. P., 1951: Annotated bibliography on condensation trails behind aircraft. — Meteorol. Abstracts and Bibliogr., Part II, Lancaster, p. 765–782.

Krastanow, L., 1940: Über die Bildung der unterkühlten Wassertropfen und der Eiskristalle in der freien Atmosphäre. — Meteorol. Z. **57**, 357–371.

Küttner, J., 1946: Beobachtungen an Kondensfahnen. — Z. Meteorol. **1**, 183–185.

Kuhn, P. M., 1970: Airborne observations of contrail effects on the thermal radiation budget. — J. Atmos. Sci. **27**, 937–942.

Lee, T. F., 1989: Jet contrail identification using the AVHRR infrared split window. — J. Appl. Meteorol. **28**, 993–995.

Liepert, B., P. Fabian, H. Grassl, 1994: Solar radiation in Germany — Observed trends and an assessment of their causes. Part I: Regional approach. — Beitr. Phys. Atmosph. **67**, 15–29.

Liou, K. N., S. C. Ou, C. Koenig, 1990: An investigation on the climatic effect of contrail cirrus. — Lecture Notes in Engrg., Vol. **60**, Springer, Berlin, 138–153.

Löhner, H., 1940: Eisnebelstreifen hinter Flugzeugen in großen Höhen. – Luftwissen **7**, 337–339.

Ludlam, F. H., R. S. Scorer, 1960: Cloud Study — A Pictorial Guide. — Murray, London, pp. 80.

Miake-Lye, R. C., M. Martinez-Sanchez, R. C. Brown, C. E. Kolb, 1993: Plume and wake dynamics, mixing, and chemistry behind a high speed civil transport aircraft. — J. Aircraft **30**, 467–479.

Mirabel, P., J. L. Katz, 1974: Binary homogeneous nucleation as a mechanism for the formation of aerosols. — J. Chem. Phys. **60**, 1138–1144.

Mollier, R., 1923: Ein neues Diagramm für Dampfluftgemische. — Z. VDI **67**, 869–872.

Murcray, W. B., 1970: On the possibility of weather modification by aircraft contrails. — Mon. Wea. Rev. **98**, 745–748.

NASA, 1976: U. S. Standard Atmosphere, 1976. — National Aeronautics & Space Administration, Washington, D.C., NTIS, Springfield, VA 22161, ADA 035 728, pp. 227.

Odgers, J., D. Kretschmer, 1986: Gas Turbine Fuels and Their Influence on Combustion. — Tunbridge Wells, Kent and Cambridge, Mass., pp. 182.

Peppler, W., 1930: Wolkenbildung durch Flugzeuge. — Z. angew. Meteorol. **47**, 35–46.

Peters, J. L. 1993: New techniques for contrail forecasting. — Air Weather Service, Scott Air Force Base, Illinois, AWS/TR-93/001, AD-A269 686, pp. 31.

Pilié, R. J., J. E. Jiusto, 1958: A laboratory study of contrails. — J. Meteorol. **15**, 149–154.

Pitchford, M., J. G. Hudson, J. Hallet, 1991: Size and critical supersaturation for condensation of jet engine exhaust particles. — J. Geophys. Res. **96**, 20787–20793.

Ponater, M., S. Brinkop, R. Sausen, U. Schumann, 1996: Simulating the global atmospheric response to aircraft water vapour emissions and contrails — A first approach using a GCM. — Ann. Geophys., submitted.

Pruppacher, H. R., 1995: A new look at homogeneous ice nucleation in supercooled water drops. — J. Atmos. Sci. **52**, 1924–1933.

Pruppacher, H. R., J. D. Klett, 1980: Microphysics of Clouds and Precipitation. — Reidel, Dordrecht, pp. 714.

Rango, A. L., P. V. Hobbs, 1983: Production of ice particles in clouds due to aircraft penetrations. — J. Clim. Appl. Meteorol. **22**, 214–232.

— — 1984: Further observations of the production of ice particles in clouds by aircraft. — J. Clim. Appl. Meteorol. **23**, 985–987.

Regener, E., 1941: Versuche über die Kondensation und Sublimation des Wasserdampfes bei tiefen Temperaturen. — Schriften der Deutschen Akademie der Luftfahrtforschung, Verlag R. Oldenbourg, München und Berlin, H. 37, 17–24.

Reiner, T., F. Arnold, 1993: Laboratory flow reactor measurements of the reaction $SO_3+H_2O+M \rightarrow H_2SO_4+M$: Implications for gaseous H_2SO_4 and aerosol formation in the plumes of jet aircraft. — Geophys. Res. Lett. **20**, 2659–2662.

Reinking, R. F. 1968: Insolation reductions by contrails. — Weather **23**, 171–173.

Rind, D., P. Lonergan, 1995: Modeled impacts of stratospheric ozone and water vapor perturbations with implications for high-speed civil transport aircraft. — J. Geophys. Res. **100**, 7381–7396.

Roll, O., 1990: Kondensstreifen im Satellitenbild. — Diplom-Arbeit, Inst. f. Geophys. Meteorol. Univ. Köln, pp. 117.

Sassen, K., 1979: Iridescence in an aircraft contrail. — J. Opt. Soc. Am. **69**, 1080–1083 and 1194.

— 1991: Aircraft-produced ice particles in a highly supercooled altocumulus cloud. —J. Appl. Meteorol. **30**, 765–775.

Sassen, K., G. C. Dodd, 1989: Haze particle nucleation simulations in cirrus clouds, and applications for numerical and lidar studies. — J. Atmos. Sci. **46**, 3005–3014.

Sassen, K., M. K. Griffin, G. C. Dodd, 1989: Optical scattering and microphysical properties of subvisual cirrus clouds, and climatic implications. — J. Appl. Meteorol. **28**, 91–98.

Sassen, K., K. N. Liou, S. Kinne, M. Griffin, 1985: Highly supercooled cirrus cloud water: Confirmation and climatic implications. — Science **227**, 411–413.

Schilling, V. K., 1992: Motion and decay of trailing vortices within the atmospheric surface layer. — Beitr. Phys. Atmosph. **65**, 157–169.

Schmauss, A., 1919: Bildung einer Cirruswolke durch einen Flieger. Randbemerkungen IV. — Meteorol. Z. **36**, 265.

Schmidt, E., 1941: Die Entstehung von Eisnebel aus den Auspuffgasen von Flugmotoren. — Schriften der Deutschen Akademie der Luftfahrtforschung, Verlag R. Oldenbourg, München und Berlin, H. 44, 1–15, available at Deutsches Museum Munich, DLR Göttingen, and DLR Oberpfaffenhofen. Auszug in: Jahrbuch der Deutschen Akademie der Luftfahrtforschung, 1940/1941, Berlin, 126–135.

— 1963: Einführung in die Technische Thermodynamik. — 10th ed., Springer, Berlin, pp. 559.

Schreiner, T., 1919: Flugzeuge als Wolkenbildner und Wolkenfresser. — Deutsche Luftfahrer-Z. **6**, H. 13–14, 6.

Schumann, U. (Ed.), 1990: Air Traffic and the Environment — Background, Tendencies and Potential Global Atmospheric Effects. — Lecture Notes in Engrg., Vol. **60**, Springer, Berlin, pp. 170.

— 1994: On the effect of emissions from aircraft engines on the state of the atmosphere. — Ann. Geophys. **12**, 365–384.

— (Ed.), 1995: The impact of NO_x emissions from aircraft upon the atmosphere at flight altitudes 8–15 km. — Final Report to the Commission of the European Communities, Contract EV5V-CT91-0044, pp. 471; DLR, ISBN-92-826-8281-1.

Schumann, U., P. Konopka, R. Baumann, R. Busen, T. Gerz, H. Schlager, P. Schulte, H. Volkert, 1995: Estimate of diffusion parameters of aircraft exhaust plumes near the tropopause from nitric oxide and turbulence measurements. — J. Geophys. Res. **100**, 14147–14162.

Schumann, U., J. Ström, R. Busen, R. Baumann, K. Gierens, M. Krautstrunk, F. P. Schröder, J. Stingl, 1996: In situ observations of particles in jet aircraft exhausts and contrails for different sulfur containing fuels. — J. Geophys. Res., in press.

Schumann, U., P. Wendling, 1990: Determination of contrails from satellite data and observational results. — Lecture Notes in Engrg., Vol. **60**, Springer, Berlin, 138–153.

Schumann, U., D. Wurzel (eds.), 1994: Impact of Emissions from Aircraft and Spacecraft upon the Atmosphere. — Proc. of an Intern. Sci. Colloquium, Köln, Germany, April 18–20, 1994, DLR-Mitt. 94-06, pp. 496.

Scorer, R. S., 1955: Condensation trails. — Weather **10**, 281–287.

— 1972: Clouds of the World. — Lothian, Melbourne, pp. 176.

— 1986: Cloud Investigation by Satellite. — Wiley, New York.

Scorer, R. S., L. J. Davenport, 1970: Contrails and aircraft downwash. — J. Fluid Mech. **43**, 451–464.

Seaver, W. L., J. E. Lee, 1987: A statistical examination of sky cover changes in the contiguous United States. — J. Clim. Appl. Meteorol. **26**, 88–95.

Simpson, Sir G. C., 1941: On the formation of cloud and rain. — Quart. J. Roy. Meteorol. Soc. **67**, 99–133.

Singh, S., 1992: Method of suppressing formation of contrails and solution therefore. — US Patent 5,110,502.

Sonntag, D. 1994: Advancements in the field of hygrometry. — Meteorol. Z., N.F., **3**, 51–66.

Strauss, B., 1994: Über den Einfluß natürlicher und anthropogener Eiswolken auf das regionale Klima — mit besonderer Berücksichtigung des mikrophysikalischen Einflusses. — DLR-FB 94-23, pp. 97.

Tape, W., 1994: Atmospheric Halos. — Americ. Geophys. Union, ISBN 0-87590-834-9, pp. 143.

Thuman, W. C., E. Robinson, 1954: Studies of Alaskan ice-fog particles. — J. Meteorol. **11**, 151–156.

van de Hulst, H. C., 1957: Light Scattering by Small Particles. — Wiley, New York.

van Dyke, M., 1982: An Album of Fluid Motion. — Parabolic Press, Stanford, Calif., pp. 176.

Varney, B. M., 1921: The Argonne battle cloud. — Mon. Wea. Rev. **49**, 348–349.

Volmer, M., 1939. Kinetik der Phasenbildung. — Steinkopff, Dresden und Leipzig, pp. 220.

Wall, E., 1942: Materialien zur Frage der Eiskernbildung in der Atmosphäre. — Meteorol. Z. **59**, 109–120.

Wegener, A., 1920: Frostübersättigung und Cirren. — Meteorol. Z. **37**, 8–12. English abstract in Mon. Wea. Rev. **49** (1921), 349.

Weickmann, L., 1919: Wolkenbildung durch ein Flugzeug. — Naturwissenschaften **7**, 625.

Weickmann, H., 1945: Formen und Bildung atmosphärischer Eiskristalle. — Beitr. Phys. Atmosph. **28**, 12–52.

— 1949: Die Eisphase in der Atmosphäre. — Berichte des Deutschen Wetterdienstes in der US-Zone Nr. 6, 3–54.

Winter, C.-J., 1990: Hydrogen technologies for future aircraft. — Lecture Notes in Engrg., Vol. **60**, Springer, Berlin, 23–42.

WMO, 1995: Scientific Assessment of Ozone Depletion: 1994. — Global Ozone Research and Monitoring Project — Rep. No. 37, World Meteorological Organization, C. P. No. 5, CH-1211 Geneva 20, Switzerland.

Woodley, W. L., T. J. Henderson, B. Vonnegut, G. Gordon, R. Breidenthal, S. M. Holle, 1991: Aircraft-produced ice particles (APIPs) in supercooled clouds and the probable mechanism for their production. — J. Appl. Meteorol. **30**, 1469—1489.

ZFM, 1914: Zusammenstellung der bedeutenden Rekordflüge 1908 bis 1913. — Z. Flugtechnik Motorluftschiffahrt **5**, H. 2, 29.

— 1920: Höchstleistungen. — Z. Flugtechnik Motorluftschiffahrt **9**, H. 4, 59.

Zhao, J., R. P. Turco, 1995: Nucleation simulation in the wake of a jet aircraft in stratospheric flight. — J. Aerosol Sci. **26**, 779–795.

ULRICH SCHUMANN
Deutsche Forschungsanstalt für
Luft- und Raumfahrt (DLR)
Institut für Physik der
Atmosphäre
Oberpfaffenhofen
D-82230 Weßling

Received 28 September 1995, in revised form: 6 November 1995